ARCHIVIO ISTITUZIONALE
DELLA RICERCA

Alma Mater Studiorum Università di Bologna
Archivio istituzionale della ricerca

Basin-scale stratigraphic correlation of late Pleistocene-Holocene (MIS 5e-MIS 1) strata across the rapidly subsiding Po Basin (northern Italy)

This is the final peer-reviewed author's accepted manuscript (postprint) of the following publication:

*Published Version:*
Campo B., Bruno L., Amorosi A. (2020). Basin-scale stratigraphic correlation of late Pleistocene-Holocene (MIS 5e-MIS 1) strata across the rapidly subsiding Po Basin (northern Italy). QUATERNARY SCIENCE REVIEWS, 237, 1-22 [10.1016/j.quascirev.2020.106300].

*Availability:*
This version is available at: https://hdl.handle.net/11585/806554 since: 2024-05-15

*Published:*
DOI: http://doi.org/10.1016/j.quascirev.2020.106300

*Terms of use:*

Some rights reserved. The terms and conditions for the reuse of this version of the manuscript are specified in the publishing policy. For all terms of use and more information see the publisher's website.

This item was downloaded from IRIS Università di Bologna (https://cris.unibo.it/).
When citing, please refer to the published version.

(Article begins on next page)

16 October 2026

This is the final peer-reviewed accepted manuscript of:

**Campo, B., Bruno, L., & Amorosi, A. (2020). Basin-scale stratigraphic correlation of late pleistocene-holocene (MIS 5e-MIS 1) strata across the rapidly subsiding po basin (northern italy). Quaternary Science Reviews, 237**

The final published version is available online at ***https://dx.doi.org/10.1016/j.quascirev.2020.106300***

Rights / License:

The terms and conditions for the reuse of this version of the manuscript are specified in the publishing policy. For all terms of use and more information see the publisher's website.

*This item was downloaded from IRIS Università di Bologna (https://cris.unibo.it/)*

***When citing, please refer to the published version.***

# Basin-scale stratigraphic correlation of Late Pleistocene-Holocene (MIS 5e-MIS 1) strata across the rapidly subsiding Po Basin (northern Italy)

Campo B.[1*], Bruno L.[2], Amorosi A.[1]

[1] Dipartimento di Scienze Biologiche, Geologiche ed Ambientali (BiGeA), Università degli Studi di Bologna, Piazza di Porta San Donato 1, 40126, Bologna (Italy). E-mail addresses: bruno.campo@unibo.it (* corresponding author); alessandro.amorosi@unibo.it.

[2] Dipartimento di Scienze Chimiche e Geologiche, Università degli Studi di Modena e Reggio Emilia, Via Giuseppe Campi 103, 41125, Modena (Italy). E-mail address: luigi.bruno@unimore.it.

## Highlights

- The stratigraphic architecture of the last 130 ky in the Po Basin was reconstructed
- Along-strike and along-dip facies changes are emphasized through transects
- Detailed facies mapping of the MIS 5e maximum marine ingression has been provided
- MIS 5e-MIS 1 facies architecture clearly denotes a main glacio-eustatic control
- Detailed stratigraphic correlations reveal a structural control on sedimentation

## Abstract

Eight stratigraphic transects, 40 to 140 km long reveal, for the first time on a regional scale, a comprehensive picture of facies architecture of the highly preserved Late Pleistocene-Holocene sedimentary succession from the rapidly subsiding Po Basin. Facies analysis and pollen-based correlation, supported by radiocarbon, electron-spin resonance and optically stimulated luminescence dates, enabled the attribution of distinct stratigraphic intervals to Marine Isotope Stages (MIS) 6 to 1.

Basin-scale facies changes appear to have been driven mostly by glacio-eustatic oscillations falling in the Milankovitch band (~100 ky). The MIS 5e coastal wedge was tracked continuously beneath the modern shoreline, for over 110 km along strike. Along-dip (west-east) stratigraphic correlation over 140 km revealed

the characteristic landward transition from shallow-marine and coastal facies to lagoonal, swamp, and floodplain deposits.

The MIS 5d-MIS 2 stratigraphic succession, up to 95-m-thick, records the stepped, basinward shift of facies related to the post-MIS 5e sea-level fall. In particular, lagoon and swamp facies mark minor transgressions (Substages 5c and 5a), whereas thick floodplain deposits and laterally extensive (> 40 km) fluvial channel-belts, up to 30 m thick, characterized the glacial periods (MIS 4 and MIS 2).

The Holocene (MIS 1) coastal wedge shares many similarities in terms of facies architecture and geometry with its MIS 5e counterpart, though maximum landward marine incursion during the MIS 5e transgression was 10 km farther inland (35 km inland of modern shoreline). Organic-rich (freshwater swamp) environments developed > 100 km landwards of the present-day coastline.

The MIS 5e-MIS 1 succession of the Po Basin displays an exceptional thickness, up to 130 m. Minimum values (~20 m) are recorded close to the Apennine margin and above the buried actively growing anticlines. The spatial distribution and geometry of the MIS 5e-MIS 1 strata, as well as rapidly varying subsidence rates (from 0.2 to 1.0 mm/y) reflect the strong influence of the structural setting (location of major thrust fronts) over the creation/destruction of accommodation.

**Keywords:** Late Quaternary; Last Interglacial; MIS 5e coastal wedge; Maximum marine ingression; Po Basin.

## 1. Introduction

The Last Interglacial (LI) coincides with Marine Isotope Stage (MIS) 5e, which is a proxy record of low global ice volume and high sea-level (Kukla et al., 2002). MIS 5e is the lowest substage of MIS 5 (Shackleton, 1969), which spans the time interval between Termination II (end of MIS 6,~135 ky BP) and the onset of MIS 5d (~116 ky BP; Murray-Wallace, 2013; Shackleton et al., 2003).

The MIS 5e interval was characterized by warmer climate conditions and higher global sea-level (up to 9 m) than the present interglacial (MIS 1; Antonioli, 2012; Dutton et al., 2015; Dutton and Lambeck, 2012; Kopp et al., 2009; Tzedakis et al., 2018; Waelbroeck et al., 2002). For this reason, the LI is generally considered a good analog, albeit imperfect, of possible scenarios resulting from the ongoing global warming (Antonioli et

al., 2017; Clark and Huybers, 2009; IPCC, 2018, 2007; Overpeck et al., 2006; Sánchez Goñi et al., 2012, 1999; Tzedakis, 2013) and its near-future projections (Church et al., 2013; Horton et al., 2019; Rohling et al., 2008; Stammer et al., 2019).

Climate and relative sea-level characteristics of MIS 5e have been typically reconstructed from ice and marine cores (Bard et al., 1990; Chappell and Shackleton, 1986; Chappell et al., 1996; Shackleton, 2000, 1987; Siddall et al., 2003; Waelbroeck et al., 2002). On the other hand, LI sea-level has been estimated through the analysis of geomorphological and stratigraphical features, such as prominent tidal notches, lagoonal sedimentary facies, fossil beaches and marine terraces (Lambeck et al., 2004; Murray-Wallace, 2013; Pirazzoli, 1993; Rovere et al., 2016) or submerged speleothems (Antonioli et al., 2004; Bard et al., 2002). These sea-level indicators have also been used as a regional datum to quantify geodetic variations over the last 120 ky (Bordoni and Valensise, 1998; Murray-Wallace, 2002). In general, MIS 5e deposits are worldwide considered as important stratigraphic markers (Creveling et al., 2015; Murray-Wallace and Woodroffe, 2014) and have been used to assess vertical displacements due to regional subsidence or uplift (Ferranti et al., 2010, 2006; Galili et al., 2007; Guillaume et al., 2013; Lambeck et al., 2004; Matsu'ura et al., 2019; Rovere et al., 2016). MIS 5e sea-level markers have been documented worldwide in sub-aerially exposed successions in stable or uplifting areas (Amorosi et al., 2014; Bardají et al., 2009; Carr et al., 2010; Mauz et al., 2012; Murray-Wallace et al., 2016; Oliver et al., 2018), or buried beneath subsiding coastal plains (Carboni et al., 2010; De Santis et al., 2010; Otvos, 2015, 2013).

In spite of the huge number of studies that focused on the LI sedimentary record, scarce attention has been paid, in general, to detailed stratigraphic reconstructions of facies architecture, nor accurate sedimentological studies have been undertaken on buried late Pleistocene successions. In relatively proximal (alluvial) settings, the post-MIS 5e stratigraphy is generally poorly preserved due to river incision driven by sea-level fall (Blum et al., 2013; Milli et al., 2016, 2013; Otvos, 2005; Tropeano et al., 2013; Vis et al., 2008). By contrast, detailed stratigraphic information is available for the Rhine-Meuse system (the Netherlands), a low-gradient fluvial system developed in a slowly subsiding setting (Busschers et al., 2005, 2007; Peeters et al., 2019, 2015; Sier et al., 2015). However, because of river avulsion and erosion during the last 130 ky, the MIS 5-MIS 2 stratigraphic record (up to 40 m thick), has only locally been preserved (Peeters et al., 2016,

2015). Additional high-resolution studies carried out in the Kanto and Echigo coastal plains, in Japan, have been limited to the MIS 5e or MISs 3-1 intervals (Nakazawa et al., 2017; Tanabe et al., 2013, 2009).

In the Po Basin (Northern Italy, Fig. 1), high subsidence rates (up to 2.5 mm/y over the last 1.43 My; Carminati and Di Donato, 1999) have led to the deposition of a stratigraphically extensive late Quaternary succession (Regione Emilia-Romagna and Eni-Agip, 1998; Regione Lombardia and Eni Divisione Agip, 2002). Several studies, focusing on relatively small areas or even on single cores (Amorosi et al., 2004, 1999a; Castorina and Vaiani, 2018; Fiorini, 2004; Scarponi and Kowalewski, 2004), have documented an almost continuous and highly-resolved sedimentary record of the last 140 ky. These studies documented the presence of a thick coastal sediment wedge at depths of up to 100 m. Local studies from the central Po Plain, up to 140 km landwards of the modern shoreline, showed clear changes in pollen taxa and lithofacies within a fully alluvial succession (Amorosi et al., 2008, 2001; Geological Map of Italy at 1:50,000 scale, Sheets: 187, 200, 223, 240, 255), which are interpreted to represent the abrupt change from cold (MIS 6, 4, 3 and 2) to temperate (MIS 5e and 1) climatic conditions.

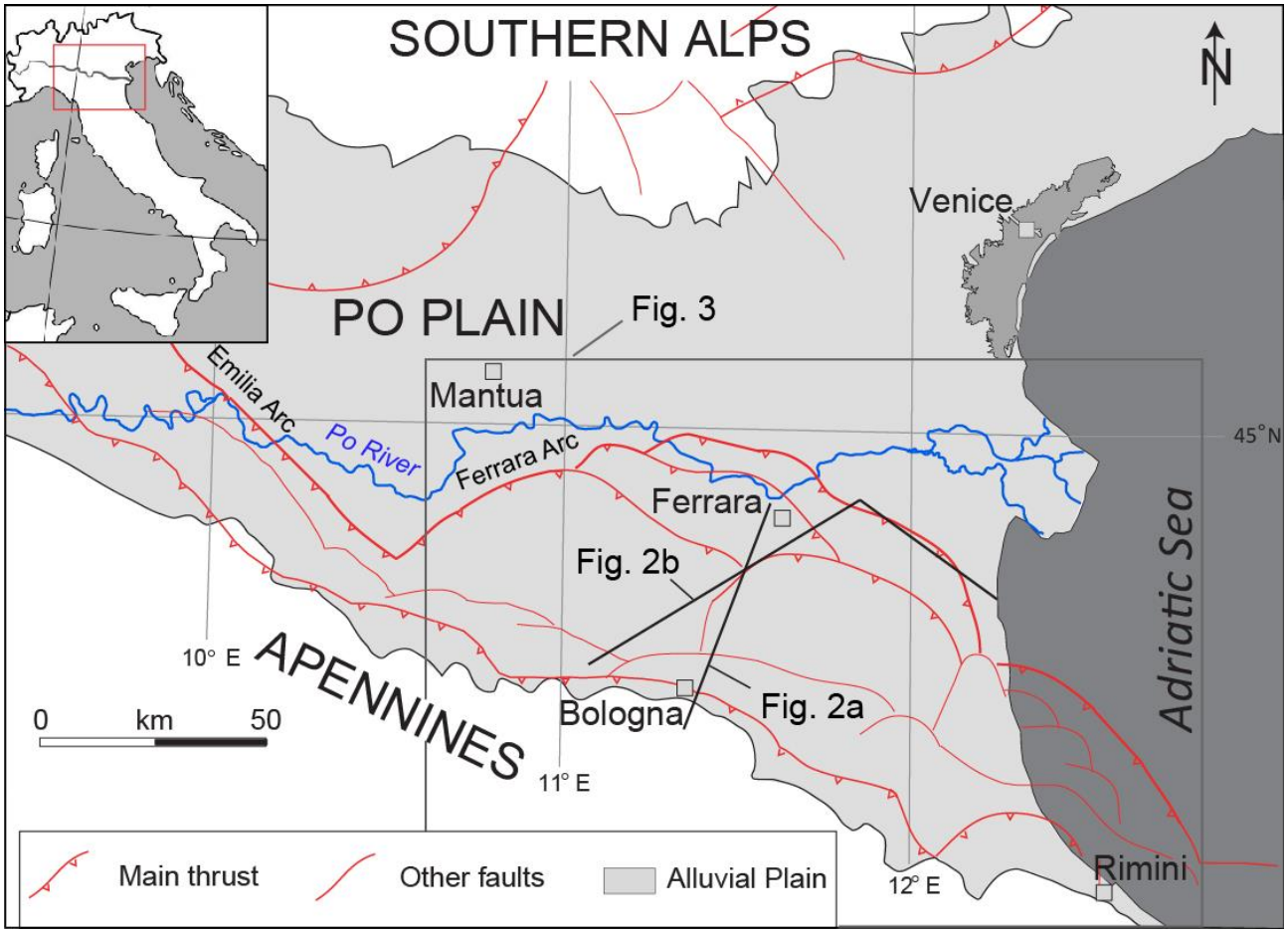

97 **Fig. 1 –** Structural map of the Po Plain, indicating the (i) buried Alpine and Apennine structures
98 (modified from Burrato et al., 2003); (ii) study area (gray rectangle), and (iii) traces of seismic and stratigraphic
99 profiles of Figure 2a, b.
100
101 Despite all these data, no stratigraphic reconstruction is currently available for the MIS 5e and post-MIS
102 5e sedimentary record at basin-scale. Whereas MIS 3-MIS 1 stratigraphy, and particularly the depositional
103 architecture of the Holocene coastal wedge, have been studied in detail (Amorosi et al., 2019, 2017a; Bruno et
104 al., 2017; Campo et al., in press, 2017), older Late Pleistocene strata are poorly known, especially in terms of
105 lateral facies distribution and geometry of sedimentary bodies.
106 This work presents, for the first time, a high-resolution reconstruction of the stratigraphic architecture
107 of the Po Basin succession of the last 130 ky. This study focusses on: (i) the basin-scale correlation of the MIS
108 5e coastal wedge and the identification of its landward equivalents; (ii) the reconstruction of its 3D geometries,
109 with a specific focus on along-dip and along-strikes facies variations; (iii) the mapping of the maximum marine
110 ingression during the MIS 5e highstand; (iv) the critical analysis of controlling-factors of facies distribution
111 and thickness of MIS 5e deposits.
112
113 **2. Geological setting**
114 **2.1 Structural setting**
115 The Po Plain is the widest alluvial plain (~ 48,000 km²) of the Italian peninsula. It is the morphological
116 expression of the Po Basin, a rapidly subsiding basin bounded by the south-verging Southern Alps and the
117 north-verging Northern Apennines (Burrato et al., 2003; Fig. 1). These two orogens started to form in the
118 Cretaceous, in response to the collision of the Adria microplate and the European Plate (Carminati and
119 Doglioni, 2012). The Northern Apennines are a fold-and-thrust belt that formed mostly during the Neogene
120 and the Quaternary (Basili and Barba, 2007; Malinverno and Ryan, 1986; Royden et al., 1987). The most
121 external thrusts of the Apennines are buried beneath the Miocene to Quaternary sedimentary infill of the
122 southern Po Basin (Pieri and Groppi, 1981; Figs. 1, 2a). In the central and eastern sectors of the Po Plain, the
123 buried structures of the Northern Apennines consist of two arched thrust systems, with convexity towards the
124 NNE (Fig. 1): the Emilia arc to the W and the Ferrara arc to the SE (Fig. 1). These thrust systems became

active in the Late Miocene (Boccaletti et al., 2011; Picotti and Pazzaglia, 2008; Scrocca et al., 2007) and, following the 2012 seismic events in the southern Po Plain (i.e. Emilia Earthquake, 2012; Caputo et al., 2015; Pondrelli et al., 2012) they are considered to be still active. Fault propagation and imbrication led to the formation of thrust-related anticlines (Maesano et al., 2015; Ori and Friend, 1984; Rossi et al., 2015; Toscani et al., 2014). Far away from anticline culminations, subsidence rates have been estimated to be as high as 2.5 mm/y over the last 1.43 My (Carminati et al., 2003; Carminati and Di Donato, 1999).

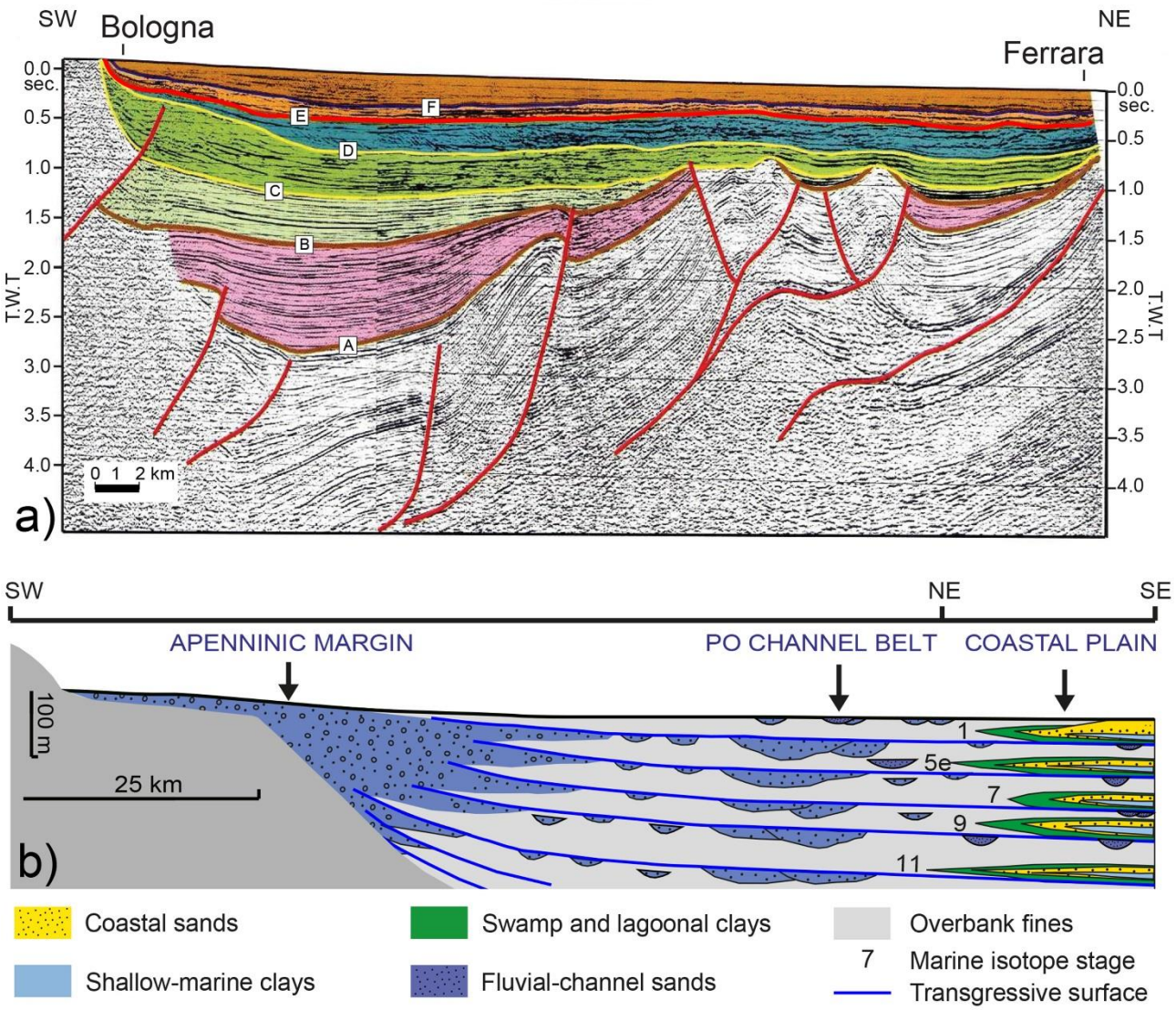


**Fig. 2 –** a) Interpreted seismic profile showing the Plio-Quaternary sedimentary infill of the Po Basin (colored area): depositional sequences (P2, Qm and Qc), major blind thrusts (red lines) and stratigraphic unconformities (A-F lines) are shown as interpreted by Regione Emilia-Romagna and ENI-Agip, (1998; location in Figure 1). T.W.T. – two-way travel time. For a depth-version of the same seismic profile, see Boccaletti et al. (2011), their Fig. 5, cross-section D-D'. b) Schematic illustration of the proximal-to-distal

stratigraphic architecture of the Middle-Late Pleistocene Po Plain succession, showing distinct cyclic changes in facies and channel stacking in the Milankovitch band (~ 100 ky). Modified from Amorosi and Colalongo (2005). Location can be found in Figure 1.

### 2.2 Stratigraphic setting

The sedimentary infill of the Po Basin has been investigated at basin-scale through the integration of seismic and well data (Amadori et al., 2019; Ghielmi et al., 2013; Pieri and Groppi, 1981; Regione Emilia-Romagna and Eni-Agip, 1998; Regione Lombardia and Eni Divisione Agip, 2002). The Plio-Quaternary succession ranges in thickness between 8 km in the depocenters, to a few hundred meters atop the buried anticlines (Mariotti and Doglioni, 2000; Pieri and Groppi, 1981). It is characterized by a shallowing-upward trend, from Pliocene deep-marine to Quaternary shallow-marine and continental deposits (Ori, 1993; Ricci Lucchi et al., 1982). Based on magnetostratigraphic data (Muttoni et al., 2003), the uppermost ~800 m of the basin fill has been dated to the last 0.87 My. Throughout the basin, from proximal to distal locations, the late Quaternary succession of the Po Basin fill is characterized by vertical cyclic changes in facies, with channel stacking-patterns reflecting the Middle-Late Pleistocene alternation of glacial and interglacial periods (Amorosi et al., 2008, 2004, 1999a). Beneath the coastal sector, two wedge-shaped, coastal to shallow-marine sediment bodies, identified around -100 m and 30 m depth (Fig. 2b) have been assigned to MIS 5e and MIS 1 respectively (Amorosi et al., 2004; Ferranti et al., 2006). Close to the Apennine margin and beneath the modern Po River, sheet-like fluvial channel-bodies were formed during glacial periods, which alternate with mud-dominated intervals assigned to the interglacials (Amorosi et al., 2008).

## 3. Materials and methods

### 3.1 Stratigraphic dataset

The study area is a ~8,500 km² wide sector of the Po Plain, framed between the cities of Mantova, Ferrara, Reggio Emilia, Bologna, and Rimini (Fig. 3). The stratigraphic reconstruction of the Late Pleistocene-Holocene succession – with a thickness of up to 150 m - has been carried out through the analysis and interpretation of a large stratigraphic dataset (Fig. 3), mostly recovered as part of the geological mapping (CARG) project of Italy (scale 1:50,000).

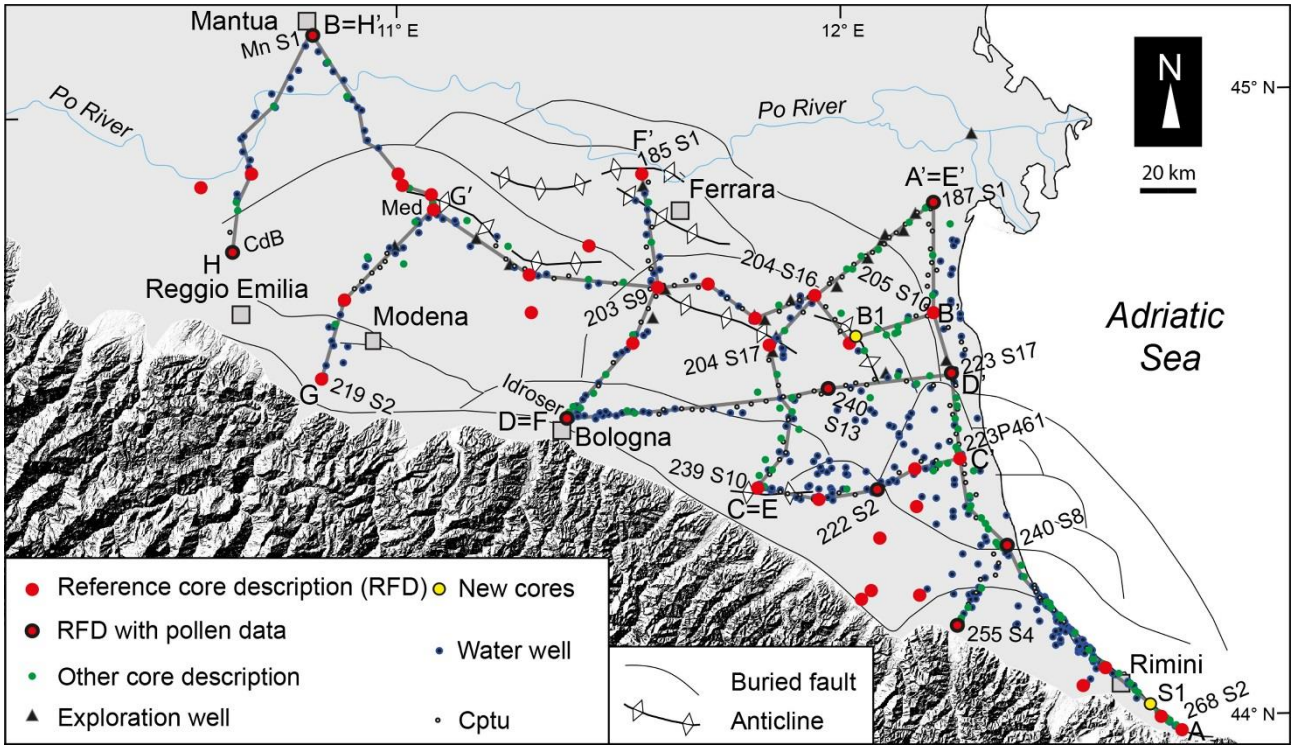


**Fig. 3 –** Study area, with indication of stratigraphic data used in this study and the main buried Apennine structures. Traces of cross sections of Figures 6-8 are represented by gray lines.

Stratigraphic data were provided by the geological surveys of Regione Emilia-Romagna and Regione Lombardia, and consist of 160 continuous-core descriptions, 554 water-well logs, 21 hydrocarbon exploration-well reports and 141 piezocone tests (see Data Availability). .

Descriptions from cores reaching depths of 30-200 m (Fig. 3), provide high-quality information about lithology, grain size, color, pedogenic and other featuressuch as peat layers, shell fragments, bioturbation, carbonate nodules, wood, and plant remains. Pocket penetration test values are frequently available. Selected core descriptions are part of published studies (Amorosi et al., 2008, 2004, 2001, 1999a; Bondesan et al., 2006; Castorina and Vaiani, 2018; Ferranti et al., 2006; Fiorini, 2004; Geological Map of Italy at 1:50,000 scale, Sheets: 256, 255, 241, 240, 223, 222, 221, 220, 205, 204, 187) and include sedimentological, micropaleontological, palynological and chronological data (i.e. $^{14}C$ and electron-spin resonance "ESR"; see Table 1 in Appendix and Data Availability). Among these, 44 cores with depths of > 100 m, have been used as reference (Fig. 3) for the identification of MIS 5e deposits and for detailed characterization of the post-MIS 5e succession.

Two continuously-cored boreholes (S1 and B1; see Fig. 3 for location), penetrating the entire MIS 5e-MIS 1 succession, were recently recovered close to the Apennine margin (core S1) and above the crest of a growing anticline in the Ferrara coastal plain (core B1; Fig. 3). Water wells (average depth ~ 150 m; Fig. 3) provided mostly basic lithological information (sand vs mud). Occasionally, the presence of marine shells is reported.

Hydrocarbon-well reports (average depth ~ 500 m; Fig. 3) provide the lowest-resolution stratigraphic information. Nevertheless, they offer petrophysical data that can be useful for lithological distinctions and, in a few cases, information about fossil and organic matter content is provided. Given their limited depth (< 35 m), piezocone tests (CPTU; Fig. 3) were utilized for stratigraphic correlation of the uppermost Pleistocene-Holocene (MIS 3-MIS 1) deposits. The reader is referred to Amorosi and Marchi, (1999), Amorosi et al., (2015) and Campo et al. (in press) for stratigraphic interpretation of CPTU tests.

### 3.2 Luminescence and radiometric dating

One undisturbed sample was collected from core B1 and sent to the Oxford Luminescence Dating Laboratory (University of Oxford, UK) for Optically Stimulated Luminescence (OSL) dating. This sample was recovered during drilling operations with an Osterberg cell from a depth of 39.9-39.3 m. The 60 cm core segment was removed and the exposed top and bottom parts were sealed with paraffin. Paraffin caps were removed in a dark room and the upper and lowermost ~5 cm of the sample were discarded. The innermost part of the core segment (39.85-39.5 m depth) was in turn split into four samples stored in lightproof containers and sent to the laboratory. At the laboratory, the samples were given the following laboratory codes:

i) X7339 (OSL sample), from core B1 (39.60-39.50 m depth);

ii) X7340 (OSL spare sample), from core B1 (39.75 m depth);

iii) X7341 (dosimetry sample), from core B1 (39.80 m depth);

iv) X7342 (dosimetry sample), from core B1 (39.85 m depth).

The resulting age is based on luminescence measurements of sand-size quartz (150-255μm) extracted from the samples using standard preparation techniques including, wet sieving, HCl (10%) treatment to remove carbonates, HF treatment (48%) to dissolve feldspatic minerals and heavy mineral separation with sodium polytungstate. Measurements were performed on small multigrain aliquots (n=30) with standard automated

luminescence readers made by Risø (Bøtter-Jensen, 1997, 1988; Bøtter-Jensen et al., 2000) and Freiberg Instruments (Richter et al., 2015) using a double SAR post-IR blue or post-IR green OSL measurement protocol (Banerjee et al., 2001; Murray and Wintle, 2000; Wintle and Murray, 2006). Dose rate calculations are based on Aitken (1985) and are derived from the concentration of radioactive elements (potassium, rubidium, thorium and uranium) within the sediment sample. These were derived from elemental analysis by ICP-MS/AES using a fusion sample preparation technique. The final OSL age estimate includes an additional 4% systematic error to account for uncertainties in source calibration and measurement reproducibility. Dose rate calculations were obtained using dose rate conversion factors of Guérin et al. (2011) and calculated using the DRAC software (v1.02) developed by Durcan et al. (2015). The contribution of cosmic radiation to the total dose rate was calculated as a function of latitude. Altitude, burial depth and an average over-burden density of 1.9 g/cm$^3$ is based on data by Prescott and Hutton (1994).

Two organic-rich samples were collected from core B1 for radiocarbon analysis. Samples were dried at 40 °C and underwent to acid-alkali-acid pretreatment before AMS counting at KIGAM Laboratory (Korea Institute of Geoscience and Mineral Resources, Daejeon, Republic of Korea). OxCal 4.2 (Ramsey and Lee, 2013) with the IntCal 13 curve (Reimer et al., 2013) was used for radiocarbon age calibration.

## 4. Depositional facies associations

The complete MIS 6-MIS 1 succession of the southern Po alluvial and coastal plain was penetrated by cores S1 and B1, respectively 55 m and 39.9 m in length (Fig. 4). Lithofacies assemblages have been extensively described in previous studies and will not be reiterated here in detail. For detailed facies analysis of the MIS 6-MIS 3 interval, the reader is referred to Amorosi et al. (2008, 2004, 2001, 1999a) and Bondesan et al. (2006); whereas, for the MIS 2-MIS 1 interval, high-resolution facies descriptions have been reported by Amorosi et al. (2017a, 2017b), Bruno et al. (2017), and Campo et al. (2017). As documented by these studies, a large variety of facies associations typifies the MIS 6-MIS 1 Po Plain succession. For a complete overview of their major characteristics the reader may refer to the table in the Appendix. A generalized description of these deposits is given below. Twenty-one facies associations were grouped into five main depositional systems. Each group is briefly described from proximal to distal locations.

- Alluvial plain deposits. Three main facies associations form the alluvial plain depositional system: the fluvial-channel facies association is 2-30 m thick, and consists of fine to coarse sand, up to gravel bodies with fining-upwards (FU) trends (Fig. 4) and erosional lower boundaries. Crevasse and levee facies are made up of < 2 m thick sand bodies and sand-silt alternations, respectively (Fig. 4), with scattered root fragments. FU trends and sharp lower boundaries are characteristic of crevasse channels; in contrast, crevasse splays show coarsening-upward (CU) grain-size trends and gradational lower boundaries. The well-drained floodplain facies association is characterized by rooted and bioturbated clay and silty clay deposits with brownish mottles. Pedogenic features typical of weakly developed paleosols (Inceptisols; Fig. 4) are common. The occurrence of meiofauna commonly is rare, and includes fragments of freshwater (F) ostracods and poorly-preserved marine foraminifers, mostly sparse in sandy deposits. Freshwater gastropods are locally encountered (Fig. 4).

- Freshwater and organic-rich inner/wave-dominated estuarine deposits. This depositional system includes five freshwater (F), hypoaline and locally organic-rich facies associations (Fig. 4). Distributary-channel (Fig. 4) and related crevasse/levee facies associations share several characteristics with their alluvial counterparts: i.e. lithology, grain-size trends and erosional to transitional lower boundaries. However, distributary-channel deposits are thinner and generally finer-grained than fluvial-channel sand bodies. The bay-head delta facies association resembles distributary-channel sands in terms of lithology and sedimentary structures, but the abundance of plant debris, the local development of CU trends, and the association between freshwater and brackish fossils may represent diagnostic features. The poorly-drained floodplain facies association consists of gray clay and silty clay, with no pedogenic features (Fig. 4) and rare carbonate concretions. The swamp facies association is characterized by dark to brown clay, with abundant peat, wood fragments, and vegetal remains (Fig. 4). Pedogenic features are almost absent, with the only exception of histosols. The concentration of freshwater ostracods progressively increases from poorly-drained floodplain to swamp facies. Pocket penetrometer values (Fig. 4) have commonly been used for the differentiation of fine-grained deposits within the MIS 2-MIS 1 succession (e.g. well-drained floodplain, poorly-drained floodplain, and swamp clays, see Amorosi et al., 2015). This approach, however, can locally be adopted even for their older (MIS 6 to MIS 3, Fig. 4) counterparts, when they are not already overconsolidated.

- Brackish outer wave-dominated estuarine deposits. This depositional system is composed of four mud-dominated facies associations, with a diagnostic brackish fauna (B in Fig. 4), which is tolerant to sudden

changes in salinity and organic matter content. Facies subdivision is based on (i) the frequency and thickness of sand intercalations, both increasing seawards; (ii) ostracod and foraminifer associations that reflect an increasing marine water influence downstream; (iii) organic matter concentration that increases landwards. From proximal to distal locations, brackish facies associations correspond to the following sub-environments: salt-marsh, mud-flat, central lagoon/bay and outer lagoon/bay.

- Transgressive barrier, strandplain, and delta front deposits. This depositional system includes four facies associations characterized by a generally high sand content. Grain size, ~~set (?)~~ thickness range, facies boundaries, and fossil content are the main diagnostic features: the transgressive sand-sheet facies association is the result of the shoreface retreat during MIS 5e-MIS 1 transgressions, and consists of shell-rich, medium-to-silty sands with a maximum thickness of 2 m, an erosional lower boundary and FU trends; the upper shoreface/foreshore facies association includes medium to coarse sand-bodies (1-5 m thick), with a gradational lower boundary; the lower shoreface facies association also shows transitional lower boundaries to the underlying prodelta facies and is composed of fine to very fine sand-bodies, 1-5 m thick; the mouth bar facies association, up to 10 m thick, includes medium to fine sand deposits, with an abundance of plant debris (Fig. 4). The transgressive sand-sheet facies includes reworked sediments, with a reworked microfauna and an abundance of mixed marine and brackish mollusk species (R in Fig. 4). Within mouth-bar and upper shoreface/foreshore facies, no foraminifers or ostracods are generally preserved and a paucity of shells is recorded. On the contrary, an abundant and highly diverse marine fossil assemblage (M in Fig. 4) is typical of nearshore facies: i.e. especially lower shoreface.

- Offshore/prodelta deposits. This mud-dominated depositional system represents the most distal portion of the Po Basin succession recovered onshore. Five facies associations were grouped into this depositional system. All these facies include marine (M) fossils assemblages. Fine sand-clay alternations are characteristic of the most proximal facies associations, such as the delta-front transition and offshore transition deposits. These facies associations accumulated in similar water depths but in different subenvironments characterized by high (i.e., delta-front transition) vs low/none (i.e., offshore transition) river influence, as the distance from the river mouth increases. Delta-front transition facies may include plant debris. Seawards, the sand/mud ratio rapidly decreases and organic-matter content increases: proximal prodelta facies (silty clay) is progressively replaced by distal prodelta facies (clay), up to 8 m thick. The offshore facies association is made up of

bioturbated clay deposits, up to 2 m thick. The highly diversified meiofauna, typical of open-marine conditions, and lithological characteristics are consistent with the relatively deep depositional environment. Offshore-transition deposits are characterized, instead, by less diversified assemblages; whereas, prodelta muds generally include opportunistic species able to tolerate stressed marine conditions (i.e. high freshwater and sediment inputs) related to river floods.

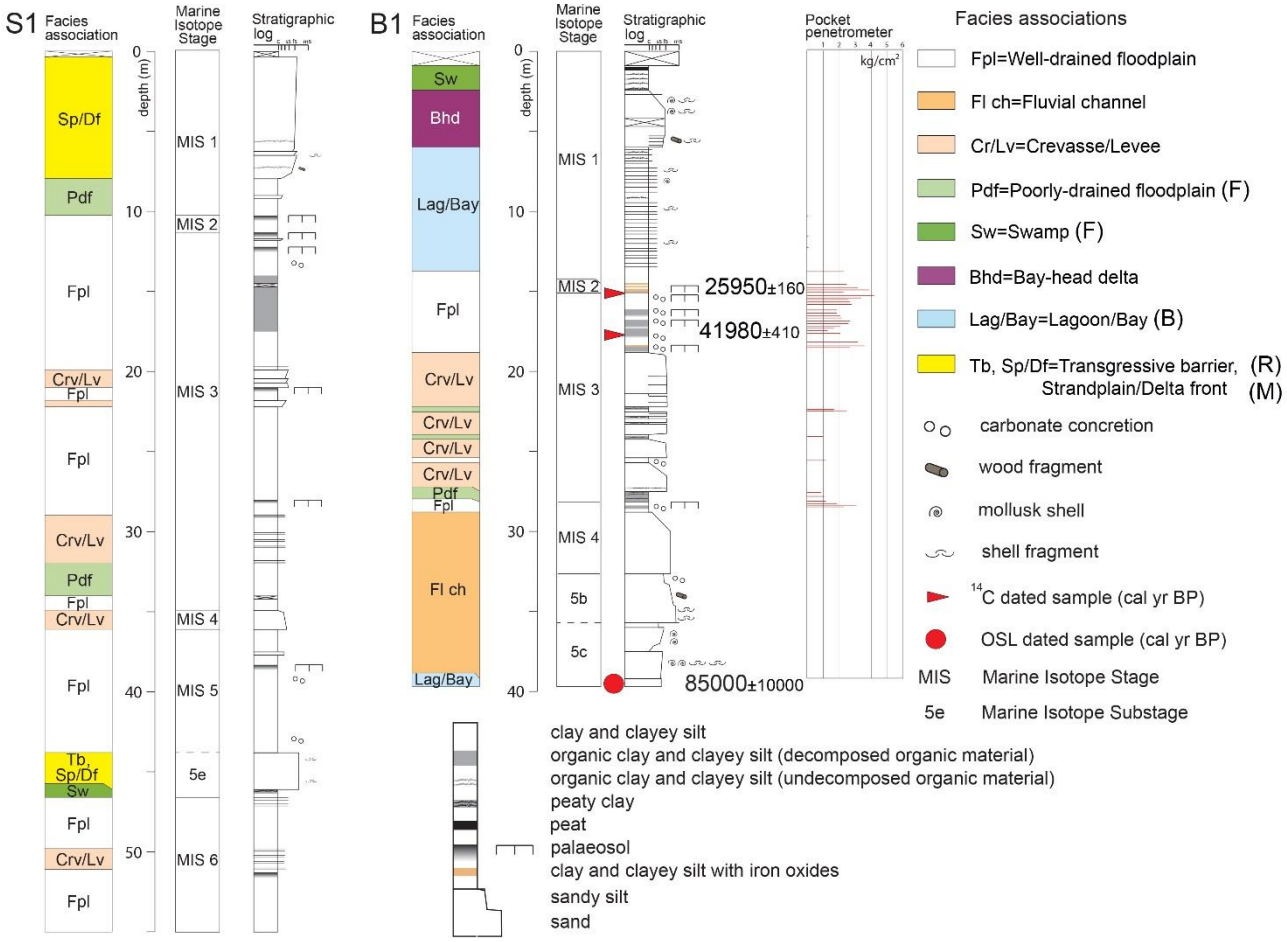


**Fig. 4** – Stratigraphic log and facies associations from cores S1 and B1. Location in Figure 3. F: freshwater; B: brackish; R: reworked; M: marine.

## 5. Pollen-based stratigraphic correlations

Stratigraphic correlations relied upon the combination of facies and pollen data available for 9 cores (Fig. 3). Particularly pollen data provided important information about climate-related vegetational and environmental changes.

Pollen taxa subdivision follows their ecological and climatic affinities (i.e. arboreal vs non arboreal and warmth- vs cold-loving taxa; see Zangheri, 1976; Pignatti, 1998, 2017), as previously done by Amorosi et al.

(2008, 2004, 2001,1999a). Two main groups have been distinguished: arboreal (AP) and non-arboreal pollen (NAP). AP can be subdivided into three components: (i) *Quercus* group, representative of warm-temperate phases (interglacials), which includes humidity- and warmth-loving species of deciduous broad-leaf forests dominated by oaks; (ii) mountain trees and (iii) *Pinus* which are indicative of cool-wet and cold climate conditions (glacials), respectively. NAP (i.e. shrubs and herbs), withstanding dry conditions, are indicators of cold steppic environments.

Vertical changes in facies associations and pollen spectra led to high-resolution stratigraphic correlations and subdivision into sediment units deposited during specific Marine Isotope Stages. Basin-scale correlations between three reference cores, representative of proximal (core Mn S1), intermediate (core 203 S9), and distal (core 223 S17) locations of the Po Basin are shown in Figure 5. A schematic stratigraphic log with facies interpretation is provided for each core. Detailed palaeontological analyses are available for cores 203 S9 and 223 S17 (Geological Map of Italy at 1:50,000 scale, Sheet: 203; Amorosi et al., 1999a), whereas pollen data were obtained from cores Mn S1, Idroser (projected on core 203 S9) and 223 S17 (Amorosi et al., 2008, 2001, 1999a).

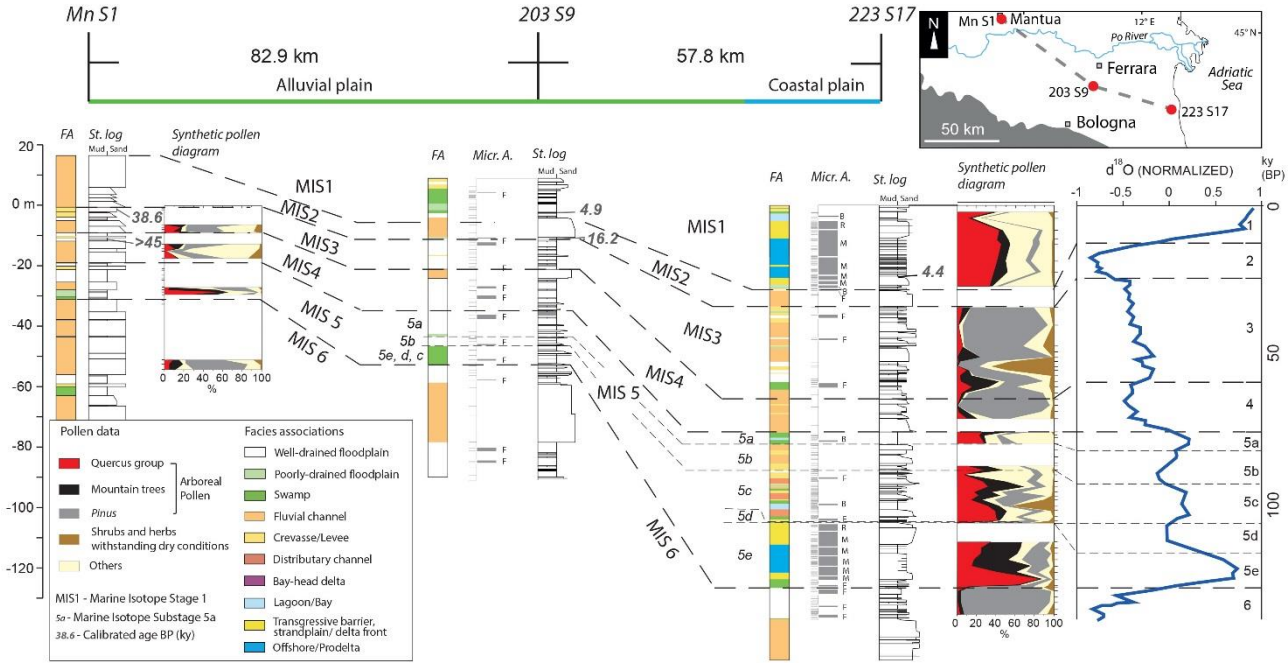


**Fig. 5** –Basin-scale correlation from proximal (alluvial plain) to distal (coastal plain) locations of the Po Basin. Facies associations and pollen signals recorded from cores were correlated with the oxygen-isotope ($\delta^{18}O$) record of the last 150 ky (blue line; modified from Martinson et al., 1987). FA: facies association; St. log: stratigraphic log; Micr. A.: Micropaleontological association (F: freshwater; B: brackish; R: reworked; M:

326 marine). See Figure 3 for location of the cores, and Table A1 (Appendix) for details on radiocarbon dates. For
327 the original pollen data the reader may refer to Data Availability.
328
329 As pollen concentration is very scarce in sandy deposits, the pollen curve from core Mn S1 is highly
330 discontinuous (Amorosi et al., 2008). However, pollen profiles from cores Mn S1, 203 S9 (i.e., Idroser) and
331 223 S17 show comparable pollen spectra at specific stratigraphic intervals (Fig. 5). Peaks in *Quercus* highlight
332 the onset of warmer/temperate periods on a basin scale. Two major warm phases were identified and linked to
333 the major peaks in $\delta^{18}O$ during MIS 5e and MIS 1 (Martinson et al., 1987, Fig. 5). The transition from glacial
334 to interglacial periods (e.g., MIS 6/5e) is characterized by sharp changes in pollen taxa (Fig. 5; Amorosi et al.,
335 2004) from high *Pinus* and mountain trees percentages (cold indicators) to high *Quercus* percentages (warm
336 indicators).
337 Pollen variations at glacial/interglacial transitions are paralleled by abrupt facies variations that reflect
338 rapid sea-level rise (Fig. 5). As an example, well-drained floodplain muds assigned to the MIS 6 glacial are
339 typically overlain by interglacial paralic and coastal facies associations attributed to MIS 5e (Fig. 5).
340 Landwards of the line of maximum marine ingression (core Mn S1, Fig. 5), the same pollen signal is associated
341 with the abrupt shift from barren fluvial sands to overlying ("transgressive") swamp muds.
342 The correlation of stages and substages relies upon similar changes in pollen signals and on vertical
343 stacking patterns of facies, with an additional contribution by radiocarbon ages for the MIS 3-MIS 1 interval
344 (Fig. 5). Minor transgressions correlate with minor peaks in $\delta^{18}O$ (MIS 5c and 5a in Fig. 5). The thick alluvial
345 succession sandwiched between MIS 5e and MIS 1 deposits, and mostly characterized by cold pollen
346 signatures can be assigned to MIS 4-3-2 (Fig. 5). Poorly-drained and swamp deposits within this interval may
347 reflect lower magnitude transgressive pulsations mostly recorded at the onset of MIS 3 (Fig. 5).
348
349 **6. MIS 5e-MIS 1 stratigraphy in the southern Po Basin**
350 Basin-scale correlations along eight stratigraphic transects (Figs. 6-8) document the high-resolution,
351 Late Pleistocene-Holocene facies architecture of the Po Plain. Pollen data, coupled with ESR, OSL and
352 radiocarbon ages enable age attribution of the investigated strata, and their assignment to the MIS 5e-MIS 1
353 interval.

Two > 100 km-long stratigraphic transect were constructed: AA' (Fig. 6a) extends from the Apennine margin to the modern Po Delta and is approximately parallel to the modern shoreline; and BB' (Fig. 6b) which runs parallel to the Apennine margin, extends from the town of Mantua to the Adriatic coast (Figs. 3, 6). Figure 7 includes three stratigraphic cross-sections (i.e. CC', DD' and EE') that were traced in the distal sector of the study area. The south-north oriented stratigraphic transects of Figure 8 (i.e. FF', GG', HH') were constructed to explore along-strike changes in stratigraphy at proximal locations.

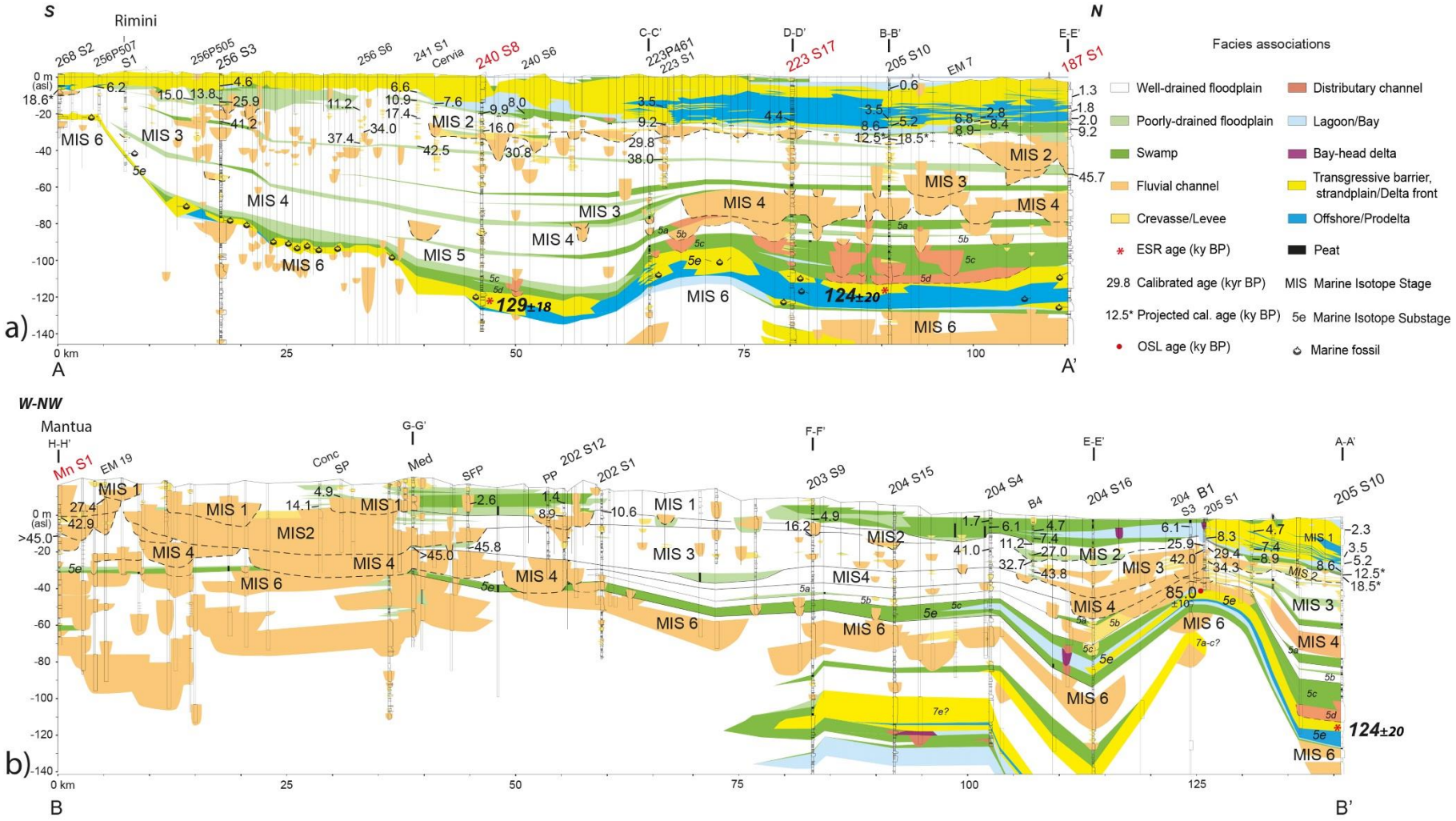
S
Rimini
N
268 S2
256P507 S1
256P505
256 S3
256 S6
241 S1 Cervia
240 S8
240 S6
C-C'
223P461
223 S1
D-D'
223 S17
B-B'
205 S10
EM 7
E-E'
187 S1
Facies associations
Well-drained floodplain
Poorly-drained floodplain
Swamp
Fluvial channel
Crevasse/Levee
ESR age (ky BP)
29.8 Calibrated age (kyr BP)
12.5* Projected cal. age (ky BP)
OSL age (ky BP)
Distributary channel
Lagoon/Bay
Bay-head delta
Transgressive barrier, strandplain/Delta front
Offshore/Prodelta
Peat
MIS Marine Isotope Stage
5e Marine Isotope Substage
Marine fossil
MIS 1
MIS 2
MIS 3
MIS 4
MIS 5
MIS 6
129±18
124±20
0 m (asl)
18.6*
0 km
25
50
75
100
A
A'
a)
W-NW
Mantua
H-H'
Mn S1
EM 19
Conc
SP
G-G'
Med
SFP
PP
202 S12
202 S1
F-F'
203 S9
204 S15
204 S4
B4
204 S16
E-E'
204 S3
B1
205 S1
A-A'
205 S10
MIS2
MIS4
85.0 ±10
7a-c?
7e?
125
B
B'
b)

**Fig. 6 –** Basin-scale stratigraphic architecture of the MIS 5e-MIS 1 succession of the Po Basin along two stratigraphic panels oriented parallel to the modern shoreline (a) and to the Apennine margin (b), respectively. See Figure 3 for location and Table A1 (Appendix) for details on radiocarbon dates. In red, reference cores with pollen data (see Data Availability).

The Last Interglacial (MIS 5e) coastal wedge, encountered at depths between 130 and 20 m, represents a prominent stratigraphic marker in the late Quaternary succession (Fig. 6). It is marked at the base by a characteristic deepening-upward trend, with transition from swamp to lagoon/estuary and transgressive-barrier facies (see cores 223 S17, 205 S10, 187 S1; Fig. 6a). In the distal sector, these deposits are overlain, in turn, by offshore and prodelta muds (Figs. 6 and 7). The prodelta facies association is overlain by a laterally extensive (> 100 km), ~10 m-thick, sand sheet made up of strandplain and delta front facies (Figs. 6 and 7). MIS 5e coastal deposits wedge-out southwards (Fig. 6a) and also towards the west (Fig. 6b), where coastal sands (cores 205 S10-204 S16) are progressively replaced by thin lagoon (core 204 S4) and swamp (cores 204 S15 and Mn S1) deposits. Close to the Apennine margin, where the MIS 5e succession is composed entirely of alluvial deposits (Figs. 7 and 8), lacking pollen data, the MIS 6-5e boundary has been tentatively placed in correspondence of a paleosol (core 239 S10; Fig. 7a, c) or atop laterally extensive fluvial-channel gravels, (core 219 S2; Fig. 8b). The top of MIS 5e deposits, generally ranging between 120 and 100 m depths, is only 60-40 meters deep at the top of the buried anticlines (Figs. 6b, 7b, c; Fig. 3 for location). Locally, MIS 5e deposits have been partially (Fig. 6a) or completely (Fig. 6b) eroded by younger fluvial/distributary-channel deposits. For example, in core B1, the OSL date from a distributary-channel deposit above MIS 5e marine sands yielded an age of 85±10 ky BP (Figs. 4 and 6b), consistent with a MIS 5a to MIS 5c age attribution (Otvos, 2015).

A thick (up to 95 m) succession made up entirely of non-marine deposits overlies the MIS 5e coastal wedge (Fig. 6). It is characterized by a cyclic alternation of swamp and locally brackish (core 223 S17) deposits with alluvial facies, showing an overall shallowing-upward trend. Two thin lagoon horizons have been identified between 90-65 and 60 m depth (Fig. 7b). Paludal deposits can be tracked landwards for about 40 km (Fig. 6b). Their thickness and lateral extent decrease upsection and southwards (Fig. 6a). Similarly, poorly-drained floodplain intervals thin out upstream where they are progressively replaced by well-drained-

floodplain muds and fluvial-channel sands (Figs. 6b, 7a, b). Three laterally extensive (> 40 km) fluvial channel-belt sand bodies, up to 20 m thick, are vertically stacked in the northern sector, between 80 and 30 m depths (Fig. 6a). The deepest sand sheet has been tentatively assigned to MIS 4. The narrower (< 15 km, Fig. 6b) and thinner (~ 5 m) fluvial-channel sand body accumulated between 45 and 30 ky BP (see radiocarbon dates in Fig. 6 and Table 1). The deposition of the youngest fluvial channel-belt took place between ~ 30 and 12 ky BP (Fig. 6).

The uppermost stratigraphic interval is the Holocene coastal wedge, that was deposited during the last 10 ky BP (radiometric ages of Figs. 6-8). It shares many characteristics in terms of facies distribution and geometry of sediment bodies with its MIS 5e counterpart (Fig. 6). Similarly, it wedges out toward the west (Fig. 6b), with a landward transition from marine to alluvial deposits. A comparable upward transition from basal estuarine deposits to a laterally extensive (> 100 km) coastal sand-sheet (Fig. 6a) typifies the early Holocene succession. Middle-late Holocene deposits, however, display thicker prodelta and strandplain/delta front deposits. (Fig. 6a). The maximum upstream migration of swamp, lagoon and coastal facies associations is less pronounced for the Holocene coastal wedge than for MIS 5e deposits (Figs. 6b, 7a, b, 8a).

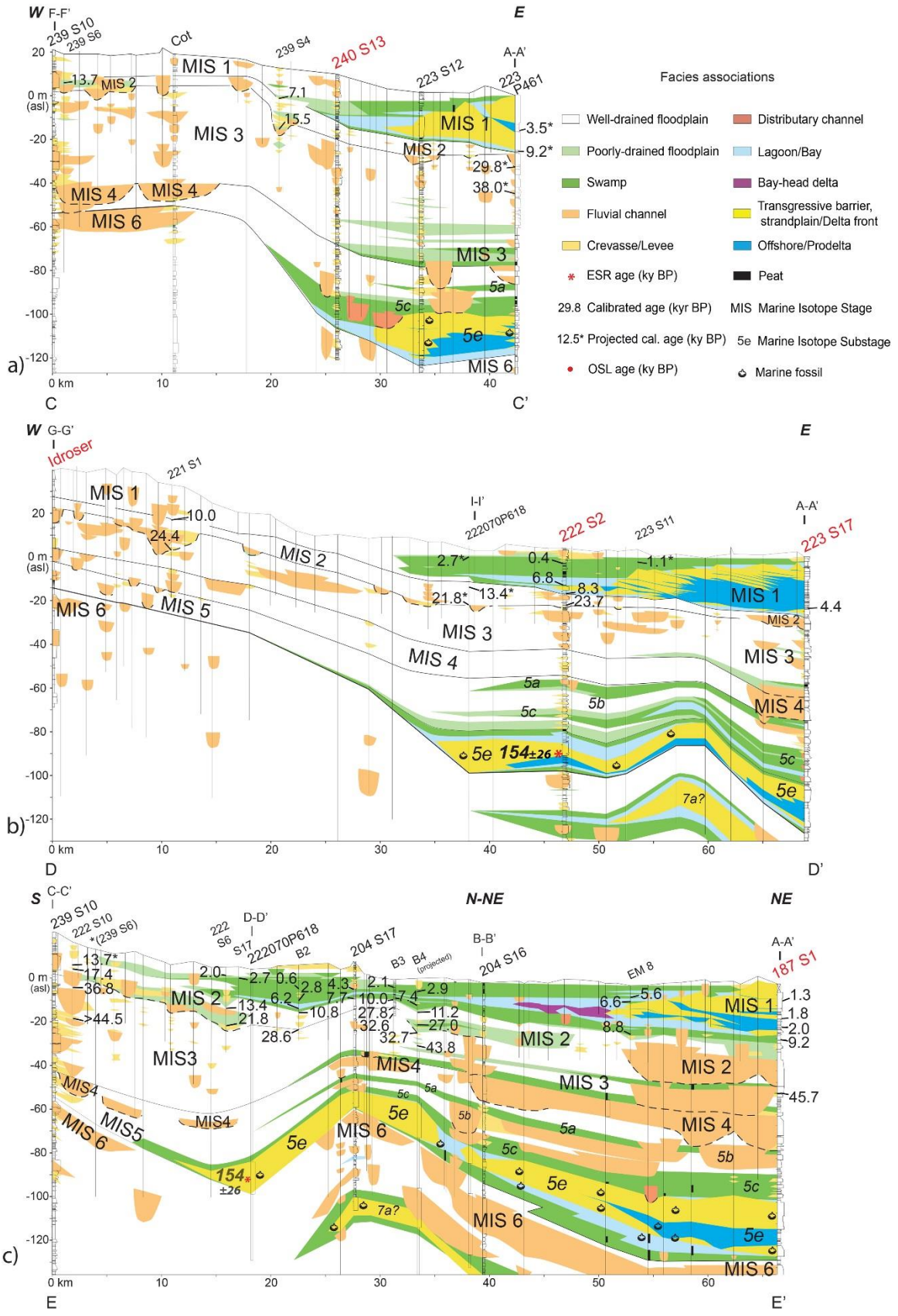


**Fig. 7 –** MIS 5e-MIS 1 stratigraphy of the Po Basin at distal locations. a) Stratigraphic panel CC'. b) Stratigraphic panel DD'. c) Stratigraphic panel EE'. See Figure 3 for location, Figure 6 for legend and Table 1 (Appendix) for details on radiocarbon dates. In red, reference cores with pollen data (see Data Availability).

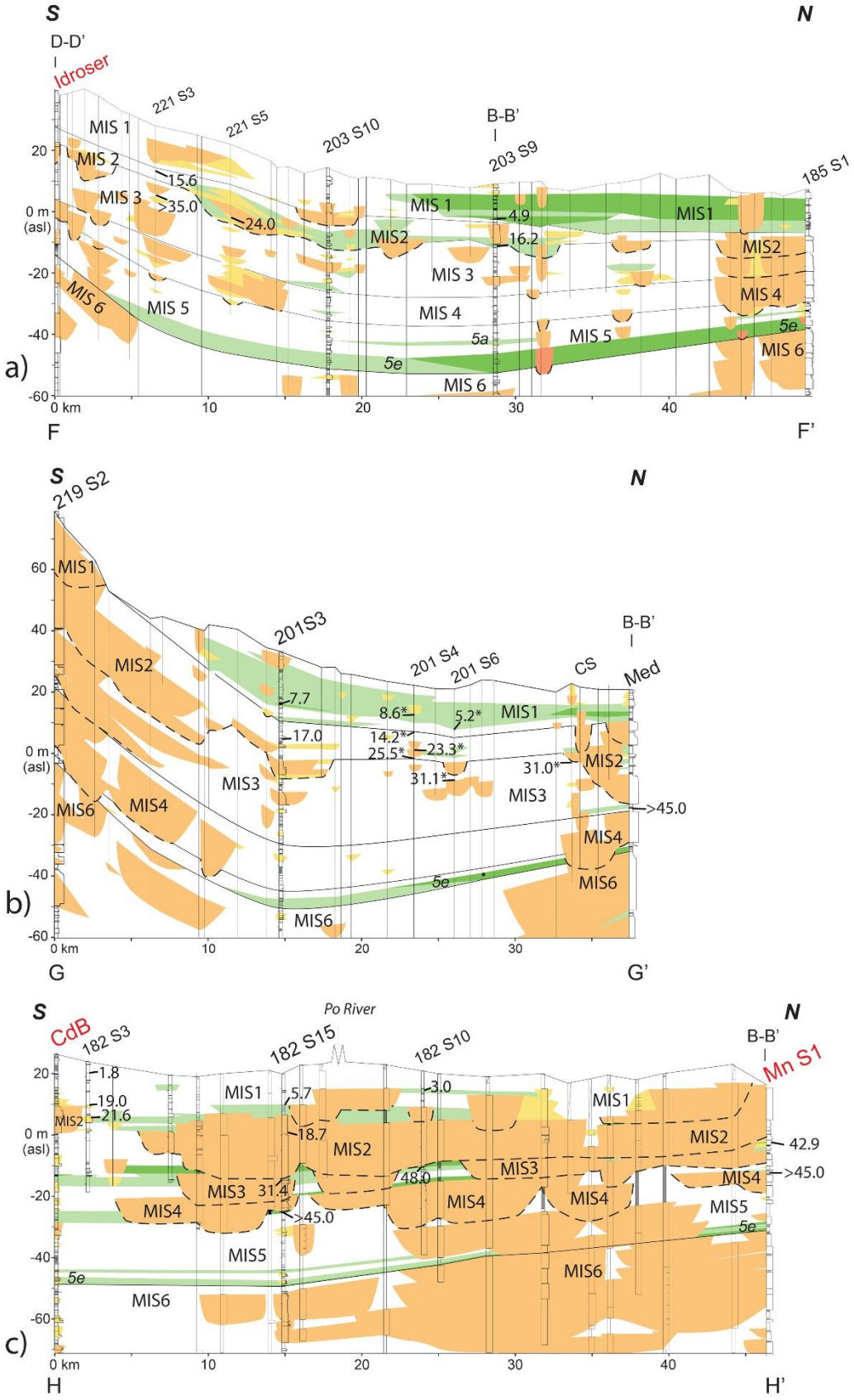


**Fig. 8 –** MIS 5e-MIS 1 stratigraphy of the Po Basin at proximal locations. a) Stratigraphic panel FF'. b) Stratigraphic panel GG'. c) Stratigraphic panel HH'. See Figure 3 for location, Figure 6 for legend and Table 1 (Appendix) for details on radiocarbon dates. In red, reference cores with pollen data (see Data Availability).

## 7. Factors controlling sediment deposition and preservation

### 7.1 Eustatic control on MIS 5e-MIS 1 stratigraphy

Facies and vegetation changes at the MIS 6/5e transition clearly reflect post-glacial sea-level rise (Waelbroeck et al., 2002). Since global mean surface temperatures were at least 2° C warmer than at present, the mean MIS 5e sea-level stood 4-6 m higher than the modern sea-level (Rohling et al., 2008), with oscillations up to 9 m (Dutton and Lambeck, 2012; Kopp et al., 2013; Rovere et al., 2016). Consequently, many coastal areas worldwide experienced the effects of a severe marine ingression (Bardají et al., 2009; Mauz et al., 2012; Murray-Wallace et al., 2016; Otvos, 2015; Peeters et al., 2019; Törnqvist et al., 2000). In the southern part of the study area (south of Ravenna in Fig. 9), the MIS 5e and MIS 1 (i.e., modern) shoreline positions approximately coincide. This is possibly due to the high topographic gradient at the basin margin that likely hindered marine transgression. On the contrary, SE of Ferrara the MIS 5e shoreline backstepped up to 36.5 km landwards of the modern beach position (9.5 km west of its MIS 1-highstand analogue - Fig. 9). Brackish lagoonal and outer estuarine environments extended up to 47.5 km from the modern shoreline, whereas more or less continuous freshwater swamp, inner-estuary environments are recorded up to 140 km upstream of the present-day coastline (Fig. 9). Poorly-drained and well-drained floodplain facies associations characterize the more abrupt transition from coastal to alluvial settings towards the Apennine margin (Fig. 9). This reconstruction is consistent with the work of Fontana et al. (2010), who placed the inner margin of the MIS 5e lagoon 10-20 km landwards of the Holocene one, in the nearby Venetian-Friulian coastal Plain.

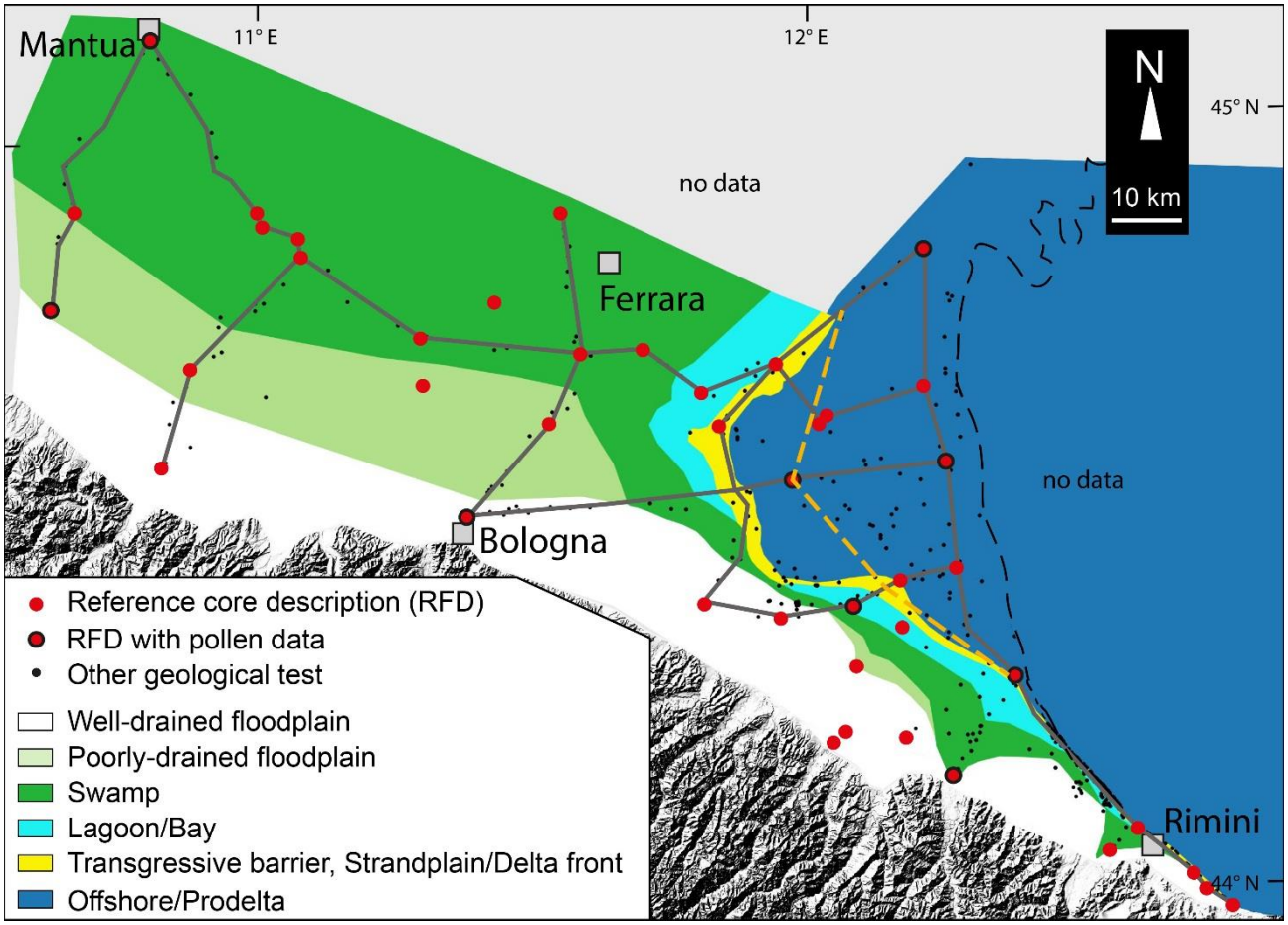


**Fig. 9** – Paleogeography of the Po Plain during the MIS 5e maximum marine ingression. Gray lines indicate the traces of stratigraphic panels of Figures 6, 7, 8. The orange dashed line depicts the MIS 1 shoreline during the MIS 1 maximum marine ingression. The black dashed-line indicates the modern shoreline.

The correlation of cyclic facies patterns and pollen signals with the oxygen-isotope record of the last 150 ky (Fig. 5) testifies to a major glacio-eustatic control on MIS 6-MIS 1 stratigraphic architecture in the Po Basin. At the scale of the last interglacial-glacial cycle (~$10^5$ years), in fact, the contribution of other allogenic (e.g., tectonics) or authogenic controlling factors on facies architecture is less clear and/or significant. Authogenic component, for example, seems to play a key-role at smaller (parasequence, $10^2$-$10^3$ years) scale, as documented by Amorosi et al. (2017, 2019). On the other hand, the exceptional stratigraphic expansion of the Po sedimentary infill, due to the high subsidence rates, allows preservation of the whole suite of Marine Isotope Stages (5 to 1) and, locally, even substages (5e-a; Figs. 6-7-8). Natural subsidence consists of a long-term component (tectonics, geodynamics, sediment load and compaction) and a short-term component due to deglaciation effects (Carminati et al., 2003, 2005). Identification of glacial and hydro-isostatic adjustment

446 component in the Mediterranean region is difficult though, especially in correspondence of major river deltas
447 (such as the Po River delta) where subsidence caused by sediment loading and compaction strongly affects the
448 relative sea level record (Vacchi et al., 2018). However, Spada et al. (2009) realized a model showing that,
449 south of the Po River, the post-LGM melting of the Alpine ice sheet reduced the sea-level rise generated by
450 the melting of the remote ice-sheet in the far-field of the Mediterranean alone. This result matches with other
451 studies (Vacchi et al., 2016; Antonioli et al., 2009) supporting a dominant role of the long-term geological
452 component of vertical deformation upon the isostatic terms in the southern Po Plain.

453 Apart from the two major transgressive pulsations, clearly marked by the two (MIS 5e and MIS 1)
454 coastal wedges, thin brackish and organic-rich intervals (Figs. 6-8) are interpreted to reflect minor
455 transgressions (i.e. MIS 5c, 5a, MIS 3) within the general sea-level fall that characterized the MIS 5e-MIS 2
456 interval. This interpretation is supported by: the i) OSL age on B1 core, dating the first non-marine sands
457 between MIS 5c and MIS 5a (Figs. 4-6b); and the ii) pollen associations from these horizons, which invariably
458 suggest phases of general climate amelioration. On the contrary, the fully alluvial MIS 5d and 5b stratigraphic
459 intervals are associated to pollen assemblages typical of colder conditions. This trend has also been observed
460 in the Rhine-Meuse system (Busschers et al., 2005; Peeters et al., 2015) and the Gulf of Mexico coastal plain
461 (Blum and Aslan, 2006; Otvos, 2005, 2013), where the re-establishment of alluvial settings is associated with
462 the switch to glacial climatic conditions. MIS 4, 3 and 2 are almost entirely composed of alluvial facies (with
463 the exception of a discontinuous, organic-rich interval assigned to MIS 3, Figs. 6-8), with pollen spectra
464 dominated by *Pinus* and mountain tree taxa. Locally, peaks of shrubs and herbs (e.g., Fig. 5) likely suggest the
465 episodic instauration of steppic environments. MIS 4 and MIS 2 intervals are characterized by two major
466 fluvial channel belts, up to 30 m thick. These laterally extensive fluvial sand bodies are coeval with vertically-
467 stacked paleosols (Figs. 6-8) that likely formed in response to abrupt sea-level falls at the transitions between
468 MIS 5/4 and MIS 3/2, respectively (Waelbroeck et al., 2002). The vertical stacking of fluvial channel-belts
469 contrasts with stratigraphy from several coastal plains worldwide, where stepped sea-level fall, down to -120
470 m at the onset of MIS 2 (Waelbroeck et al., 2002), led to the formation of well-developed incised-valley
471 systems (Blum et al., 2013; Busschers et al., 2005; Hori et al., 2002; Milli et al., 2016; Peeters et al., 2016;
472 Tanabe et al., 2013, 2006). This is likely due to high subsidence rates (~ 1 mm/y) in the Po Basin, associated

with high volumes of sediment supplied by distinct Alpine and Apennine sources (Campo et al., 2016; Fontana et al., 2014).

### 7.2 Structural control on thickness distribution

The MIS 5e-MIS 1 Po Basin succession is characterized by an exceptional thickness (up to 130 m, Figs. 6-8). Coeval successions around the world do not provide such a highly-detailed continuous sedimentary record for the last 130 ky. For example, in the marine core MD95-2042 located off the southwest coast of Portugal (Sánchez Goñi et al., 1999), the thickness of the last 130 ky sedimentary record is about 26 m. In other sedimentary successions, only distinct stratigraphic intervals are well preserved. For example, Amorosi et al. (2014) documented an uninterrupted marine sedimentary record of MIS 5e, of just 8.5 m (Fronte section, southern Italy).

Relatively thick successions have been reported from the subsurface of modern subsiding basins. In the Versilian plain (central Italy), for example, MIS 5e-MIS 1 deposits are 72 m thick (Carboni et al., 2010). However, in most alluvial systems worldwide, Late Pleistocene-Holocene strata are generally poorly-preserved due to river incision driven by stepped post-MIS 5e sea-level fall (Blum et al., 2013; Blum and Törnqvist, 2000). In the Netherlands, the MIS 5e-MIS 1 succession is preserved only within incised valleys, with thicknesses ranging between 25-60 meters along-dip (Busschers et al., 2007; Peeters et al., 2016, 2015).

In the Po Basin, the MIS 5e-MIS 1 succession has also variable thickness along-dip, between 25 and 130 meters (Figs. 6-8), where minimum values are recorded close to Apennine margin (Fig. 6a). Comparable limited thickness is also observed close to the buried growing anticlines (Fig. 6b), where the MIS 5e coastal sands can be displaced up to 70 m (Fig. 6b), and the thickness of the post-MIS 5e succession can be as little as ~ 30 m. As a whole, the general thickness distribution of the post-MIS 5e interval clearly reflects the structural setting of the Po Basin, and thus the distribution of the NNE verging fold-and-thrust systems of the Apennines (Ghielmi et al., 2013). The effect on stratigraphy of the buried Apennine structures is clearly observed between cores 205 S10 and B1 (Figs. 6b and 7c), where the thickness of the post-MIS 5e succession changes abruptly from 127 m to 51 m in about 10 km (Fig. 6b). Similarly, a change in thickness of about 30 m is recorded between well 222070P618 and core 204 S17 (Fig. 7c).

Thickness variations and deformation of stratigraphic units that compose the Plio-Quaternary Po Basin fill have been observed in numerous seismic profiles (Pieri and Groppi, 1981). In this work a significant lateral variations in thickness and deformation of Late Pleistocene strata at the subseismic-scale (Figs. 6-8)has been documented. Based on the elevation of the MIS 5e coastal sands and the modern coastal deposits, subsidence rates have been calculated dividing the MIS 5e-MIS 1 sediment thickness for the time interval (i.e., 125 ky). During the last 125 ky, subsidence ranged between 0.20 mm/y, close to the Apennine margin (in proximity of the city of Rimini), and 1.05 mm/y between the city of Cervia and the modern Po Delta (Figs. 6-9). Since the structures of the Emilia and Ferrara Arcs are tectonically active (Amadori et al., 2019), it is very difficult to rule out the possible influence of recent tectonic activity on thickness distribution and deformation of Late Pleistocene strata, with a significant contribution of differential sediment compaction.

It is possible to speculate that certain thrusts were most likely already active during the deposition (i.e., syntectonic) of the MIS 5e-MIS 1 strata. Similarly, during the last 125 ky, the study area could have been hit by several major earthquakes. These events may provoke up to 17 cm anticlinal crest growth, as shown by InSAR data analysis after the 2012-earthquake (Caputo et al., 2015). On the other hand, the interplay between sedimentary processes and high-sedimentation rates could have exceeded the velocity of the growing structures (as documented by Carminati et al., 2010 for the Mirandola area) and temporarily cover the tectonic effect (and the potential erosion) on sedimentary bodies. For example, a relative tectonic uplift of 0.16 mm/y was calculated for the Mirandola anticline (Scrocca et al., 2007), whereas the velocity of backstepping-barrier systems or delta progradation during Holocene reached 10 and 15 m/y, respectively (Bruno et al., 2017; Amorosi et al. 2019 SED).

Preexisting or new (e.g., seismogenically) generated structural highs could also have been playing a key role (morpho-tectonic?) on sediment and facies distribution, as suggested by the abrupt landward replacement of Holocene beach-barrier deposits with thick lagoonal deposits between cores 204 S3 and B1 (Fig. 6b). Given the intrinsic complexity of the geological and structural framework and the interplay between all the processes acting at different time/intensity scales, additional investigations are needed to better define and quantify the role of neo-tectonics on the MIS 5e-MIS 1 deposits of the Po Basin.

## Conclusions

Last Interglacial (MIS5e) coastal deposits represent a stratigraphic marker of worldwide significance that provides specific information about paleoclimate and paleo-sea level, and that can be used on a basin-scale to infer regional tectonics. MIS 5e strata have been reported from the subsurface of the Po Plain in several local studies, but basin-scale stratigraphic reconstructions have never been carried out. Based on 876 stratigraphic data (e.g. cores, well logs and piezocone tests), with the aid of micropaleontological, pollen, and chronological data (i.e. radiocarbon, ESR and OSL), regional stratigraphic correlation of MIS 5e deposits was established and the high-resolution facies architecture of the Late Pleistocene-Holocene succession was reconstructed with high stratigraphic detail.

The MIS 5e coastal wedge can be tracked continuously for > 100 km along strike and up to 140 km along dip. It includes the retrogradational stacking of paralic and coastal facies, overlain by prograding deltaic deposits. Coastal sands, up to 25 m thick, thin-out southwards and westwards, where they are progressively replaced by lagoon, swamp and alluvial facies.

The post-MIS 5e succession, dated between about 85 and 12 ky BP, exhibits an overall shallowing-upward trend due to the general sea-level fall: lagoon and swamp deposits are abundant atop the MIS 5e deposits, but they become thinner upsection, where alluvial facies are dominant. Stacked fluvial channel belts formed during MIS 4-2 due to the combination of high-subsidence rates and high-sediment supply. This overall trend reflects the stepped basinward shift of facies induced by sea-level drop, between MIS 5d and MIS 2. Brackish and swamp horizons are associated with minor transgressions (MIS 5c, 5a, MIS 3) within the general sea-level fall.

The Holocene (MIS 1) deposits record the post-LGM sea-level rise and subsequent Po-delta progradation under highstand conditions. The MIS 1 coastal wedge shares many characteristics in terms of pollen signals, facies trends, geometry and thickness of sedimentary bodies with its older (MIS 5e) counterpart. Due to higher global sea-level during the Last Interglacial, however, the MIS 5e shoreline reached a 9.5 km more landward position than maximum marine ingression during MIS 1: 36.5 km landwards of the modern shoreline.

The MIS 5e-MIS 1 succession displays an extremely variable thickness across the Po Basin. The exceptional thickness (~130 m) preserved in the depocenters makes the Po Plain succession one of the most extensive, continuous and highly-resolved stratigraphic records of the last 130 ky. The elevation of the MIS

5e stratigraphic marker changes dramatically on top of the major buried thrust fronts, where subsidence in the last 130 ky decreases from 1.0 to 0.2 mm/y.

**Data Availability**

- The download of geological tests used in this work is available only in Italian at the following links: https://applicazioni.regione.emilia-romagna.it/cartografia_sgss/user/viewer.jsp?service=geologia (Regione Emilia-Romagna; accessed august 2019); https://www.cartografia.servizirl.it/viewer32/index.jsp?config=config_caspita.json (Regione Lombardia; accessed august 2019).
- Pollen data are available from nine reference cores. For each core the source of data is provided:

  Core 187 S1: pollen data (only in Italian) at http://www.isprambiente.gov.it/Media/carg/note_illustrative/187_Codigoro.pdf, pages 132-133.

  Core 223 S17: pollen spectra published by Amorosi et al., 2004, 1999a.

  Core 240 S8: pollen spectra published by Amorosi et al., 2004.

  Core 255 S4: pollen spectra (only in Italian) at http://www.isprambiente.gov.it/Media/carg/note_illustrative/255_Cesena.pdf, p. 76.

  Core 222 S2: pollen spectra (only in Italian) at http://www.isprambiente.gov.it/Media/carg/note_illustrative/222_Lugo.pdf, p. 92.

  Core 240 S13: pollen spectra published by Amorosi et al., 2004.

  Core Idroser: pollen spectra published by Amorosi et al., 2001.

  Core CdB: pollen data (only in Italian) at http://www.isprambiente.gov.it/Media/carg/note_illustrative/200_Reggio_nellEmilia.pdf, pages 91-95.

  Core Mn S1: pollen spectra published by Amorosi et al., 2008.
- EPR ages for cores 205 S10, 222 S2 and 240 S8 published by Ferranti et al., 2006, page 45, their Table 2.
- Original radiometric ages from the Geological Map of Italy (only in Italian) at 1:50,000 scale (Geological Survey of Italy and CARG Project):

Sheet 182, http://www.isprambiente.gov.it/Media/carg/note_illustrative/182_Guastalla.pdf, Table 1, pp. 25-26.

Sheet 187, http://www.isprambiente.gov.it/Media/carg/note_illustrative/187_Codigoro.pdf, Table 1, p. 82.

Sheet 201, http://www.isprambiente.gov.it/Media/carg/note_illustrative/201_Modena.pdf, Table 1, p. 23.

Sheet 202, http://www.isprambiente.gov.it/Media/carg/note_illustrative/202_Giovanni_Persiceto.pdf, Table 1, p. 27.

Sheet 203, http://www.isprambiente.gov.it/Media/carg/note_illustrative/203_Poggiorenatico.pdf, Table 3, p. 24.

Sheet 204, http://www.isprambiente.gov.it/Media/carg/note_illustrative/204_Portomaggiore.pdf, Table 2, p. 22.

Sheet 205, http://www.isprambiente.gov.it/Media/carg/note_illustrative/205_Comacchio.pdf, Table 3, p. 43.

Sheet 221, http://www.isprambiente.gov.it/Media/carg/note_illustrative/221_Bologna.pdf, Table 3, pp. 45-46.

Sheet 222, http://www.isprambiente.gov.it/Media/carg/note_illustrative/222_Lugo.pdf, Table 2, p. 25.

Sheet 223, http://www.isprambiente.gov.it/Media/carg/note_illustrative/223_Ravenna.pdf, Table 1, p. 50.

Sheet 239, http://www.isprambiente.gov.it/Media/carg/note_illustrative/239_Faenza.pdf, Table 3, p. 46.

Sheets 240-241, http://www.isprambiente.gov.it/Media/carg/note_illustrative/240_241_ForliCervia.pdf, Table 4, p. 43.

Sheet 256, http://www.isprambiente.gov.it/Media/carg/note_illustrative/256_Rimini.pdf, Table 3, p. 72.

Sheet 268, the original data is available at https://applicazioni.regione.emilia-romagna.it/cartografia_sgss/user/viewer.jsp?service=geologia.

**Acknowledgements**

We are grateful to the Regione Emilia-Romagna Geological Survey for the full access to the database and for the recovery of core S1.

**Author contribution**

BC: lead author, research design, sampling campaign, geological interpretation; LB: second author, sampling campaign, geological interpretation; AA: principal investigator.

**Appendix. Supplementary data**

**Table 1 –** List of radiocarbon dates. GMI: Geological Map of Italy (see Data Availability). Proj.: projected. Frag.: fragment.

| Core | Sample depth (m) | Sample code | $^{14}$C age | Cal year BP (2σ range) | Cal year BP (mean value) | Material | Source | Figure |
|---|---|---|---|---|---|---|---|---|
| **187 S1** | 7.95 | KGM-TCa180071 | 1860±30 | 1360-1180 | 1270±90 | Shell | Amorosi et al., 2019 | 6a, 7c |
| | 15.90 | KGM-TCa180072 | 2340±30 | 1900-1690 | 1800±100 | Shell | Amorosi et al., 2019 | 6a, 7c |
| | 19.75 | KGM-TWd180579 | 2570±20 | 2180-1950 | 2070±110 | Wood | Amorosi et al., 2019 | 6a, 7c |
| | 25.85 | Beta Analytic-187 S1_25.85 | 8250±60 | 9420-9070 | 9230±170 | Plant frag. | GMI, Sheet 187 | 6a, 7c |
| | 50.05 | Beta Analytic-187 S1_50.05 | 41750±1000 | - | 45700±1900 | Peat | GMI, Sheet 187 | 6a, 7c |
| **EM 7** | 5.60 | KGM-OWd150653 | 2340±40 | 2490-2305 | 2400±90 | Wood | Amorosi et al., 2017a | 6a |
| | 19.35 | KGM-OCa150088 | 2910±40 | 2865-2530 | 2790±170 | Plant frag. | Amorosi et al., 2017a | 6a |
| | 21.30 | KGM-OCa160023 | 6430±40 | 6880-6620 | 6750±130 | Shell | Amorosi et al., 2017a | 6a |
| | 22.40 | KGM-OWd150654 | 7540±50 | 8450-8200 | 8355±120 | Plant frag. | Amorosi et al., 2017a | 6a |
| | 26.70 | KGM-OWd150655 | 8010±50 | 9050-8650 | 8860±200 | Wood | Amorosi et al., 2017a | 6a |
| **205 S10** | 5.50 | KGM-OWd170607 | 970±30 | 720-560 | 660±80 | Plant frag. | Amorosi et al., 2019 | 6a, 6b |
| | 21.75 | KGM-OCa170052 | 3750±40 | 3640-3380 | 3510±130 | Shell frag. | Amorosi et al., 2019 | 6a, 6b |
| | 25.10 | UCIAMS-51672 | 4960±15 | 5255-4985 | 5120±130 | Shell | (Scarponi et al., 2013) | 6a, 6b |
| | 29.80 | KGM-OWd170610 | 8010±50 | 8700-8420 | 8560±140 | Plant frag. | This paper | 6a, 6b |
| **205 S4** | 34.40 | ENEA-205 S4_34.4 | 15280 ± 380 | 19455–17700 | 18545±880 | Organic clay | (Amorosi et al., 2003) | 6a, 6b (Proj. 205S10) |
| **205 S14** | 31.70 | Beta analytic - 205 S14_31.7 | 10,480 ± 40 | 12570–12375 | 12430±100 | Organic clay | Amorosi et al., 2003 | 6a, 6b (Proj. 205S10) |

| | | | | | | | | |
|---|---|---|---|---|---|---|---|---|
| **223 S17** | 23.60 | ETH-50473 | 4400±35 | 4505-4230 | 4365±140 | Shell | Campo et al., 2017 | 6a, 7b |
| **223 S1** | 16.10 | LODYC-223 S17_16.1 | 3305±60 | 3645-3395 | 3535±120 | Organic clay | (Amorosi et al., 1999b) | 6a, 7a (Proj.223P461) |
| | 25.6 | LODYC-223 S17_25.6 | 8170±50 | 9270-9010 | 9130±130 | Wood | Amorosi et al., 1999b | 6a, 7a (Proj.223P461) |
| | 32.8 | LLNL-CAMS-223 S17_32.8 | 25580±170 | 30315-29260 | 29755±530 | Organic clay | Amorosi et al., 1999b | 6a, 7a (Proj.223P461) |
| | 45.00 | LLNL-CAMS-223 S17_45 | 33530±440 | 38855-36550 | 37758±1150 | Wood | Amorosi et al., 1999b | 6a, 7a (Proj.223P461) |
| **240 S6** | 21.55 | CEDAD - LTL13434A | 7384±45 | 8037-7856 | 7958±90 | Mollusk shell | Campo et al., 2017 | 6a |
| | 38.80 | KGM-OCa160036 | 26070±150 | 30780-29830 | 30350±480 | Organic clay | This paper | 6a |
| **240 S8** | 21.0 | Beta analytic - 240 S8_21 | 8840±100 | 10195-9600 | 9915±300 | Organic clay | GMI, Sheets 240-241 | 6a |
| | 30.5 | Beta analytic - 240 S8_30.5 | 13270±50 | 16145-15755 | 15955±200 | Organic clay | GMI, Sheets 240-241 | 6a |
| **Cervia** | 16.45 | KGM-OCa150092 | 6720±40 | 7665-7555 | 7585±50 | Organic clay | Campo et al., 2017 | 6a |
| **241 S1** | 10.1 | LLNL-CAMS-241 S1_10.1 | 5840±50 | 6755-6500 | 6645±130 | Organic clay | GMI, Sheets 240-241 | 6a |
| | 14.9 | LLNL-CAMS-241 S1_14.9 | 9520±50 | 10905-10655 | 10875±120 | Organic clay | GMI, Sheets 240-241 | 6a |
| | 23.7 | LLNL-CAMS-241 S1_23.7 | 14290±60 | 17610-17175 | 17400±220 | Organic clay | GMI, Sheets 240-241 | 6a |
| | 39.8 | LLNL-CAMS-241 S1_39.8 | 38390±560 | 43320-41745 | 42520±790 | Organic clay | GMI, Sheets 240-241 | 6a |
| **256 S6** | 19.9 | LLNL-CAMS-256 S6_19.9 | 9730±50 | 11245-11075 | 11145±90 | Organic clay | GMI, Sheet 256 | 6a |
| | 32.0 | ETH-256 S6_32 | 29780±320 | 34545-33375 | 33925±580 | Organic clay | GMI, Sheet 256 | 6a |
| | 38.0 | ETH-256 S6_38 | 33140±410 | 38445-36320 | 37370±1050 | Wood | GMI, Sheet 256 | 6a |
| **256 S3** | 6.6 | ETH-256 S3_6.6 | 4040±70 | 4830-4400 | 4560±220 | Organic clay | GMI, Sheet 256 | 6a |
| | 13.9 | ETH-256 S3_13.9 | 11950±85 | 14030-13560 | 13800±230 | Wood | GMI, Sheet 256 | 6a |
| | 15.4 | ETH-256 S3_15.4 | 21590±210 | 26290-25470 | 25870±410 | Wood | GMI, Sheet 256 | 6a |
| | 26.3 | ETH-256 S3_26.3 | 36800±710 | 42480-40050 | 41310±1200 | Wood | GMI, Sheet 256 | 6a |
| **256 110 P505** | 14.5 | ENEA-256P505_14.5 | 12710±150 | 15650-14370 | 15060±640 | Organic clay | GMI, Sheet 256 | 6a |
| **256 160 P507** | 7.0 | LODYC-256160P507_7 | 5335±60 | 6280-5980 | 6110±150 | Wood | GMI, Sheet 256 | 6a |
| **268 010 A501** | 7.0 | LODYC-268010A501_7 | 15385±220 | 19140-18120 | 18640±510 | Organic clay | This work | 6a (Proj.268 S2) |
| **205 S2** | 6.05 | KGM-OCa160037 | 4610±40 | 4805-4515 | 4660±140 | Shell | Amorosi et al., 2019 | 6b |
| | 10.95 | KGM-OCa170048 | 4480±40 | 4875-4640 | 4795±120 | Shell | Amorosi et al., 2019 | 6b |
| | 16.00 | KGM-OCa160038 | 7000±50 | 7480-7255 | 7370±110 | Shell | Amorosi et al., 2019 | 6b |

| | | | | | | | | |
|---|---|---|---|---|---|---|---|---|
| | 16.70 | KGM-OCa170049 | 7910±50 | 8570-8380 | 8470±90 | Shell | Amorosi et al., 2019 | 6b |
| | 18.95 | KGM-OWd170603-1 | 10960±40 | 12710-12570 | 12640±70 | Plant frag. | Amorosi et al., 2019 | 6b |
| | 19.30 | KGM-OWd170604 | 7780±40 | 8430-8220 | 8350±100 | Plant frag. | Amorosi et al., 2019 | 6b |
| | 20.50 | ENEA-205 S2_20.50 | 8400±100 | 9545-9130 | 9375±200 | Organic clay | GMI, Sheet 205 | 6b |
| | 21.15 | KGM-OWd170605 | 7970±40 | 9000-8650 | 8840±180 | Plant frag. | Amorosi et al., 2019 | 6b |
| **205 S1** | 9.80 | ETH-205 S1_9.80 | 7535±70 | 8450-8185 | 8335±130 | Shell | Amorosi et al., 2003 | 6b |
| | 14.80 | ENEA-205 S1_14.80 | 25300±180 | 29860-28870 | 29365±500 | Organic clay | Amorosi et al., 2003 | 6b |
| | 24.50 | ENEA-205 S1_24.50 | 30150±520 | 35260-33350 | 34260±950 | Organic clay | Amorosi et al., 2003 | 6b |
| **B1** | 15.1 | KGM-TSa180029a | 21690±80 | 26110-25780 | 25950±160 | Organic clay | This paper | 6b |
| | 17.7 | KGM-TSa180033a | 37590±260 | 42390-41570 | 41980±410 | Organic clay | This paper | 6b |
| **204 S3** | 4.25 | KGM-TWd180291 | 5520±40 | 6175-5935 | 6050±120 | Plant frag. | Amorosi et al., 2019 | 6b |
| **B4** | 6.05 | KGM-TWd190156 | 2770±30 | 2950-2780 | 2860±80 | Peat | This paper | 7c |
| | 8.4 | KGM-TWd190159 | 4180±30 | 4770-4610 | 4720±80 | Wood | This paper | 6b |
| | 12.4 | KGM-TWd190165 | 6470±30 | 7440-7320 | 7380±60 | Wood | This paper | 6b, 7c |
| | 15.6 | KGM-TSa190029 | 9780±60 | 11320-11080 | 11200±120 | Organic clay | This paper | 6b, 7c |
| | 21.3 | KGM-TWd190167 | 22710±90 | 27350-26690 | 27080±330 | Peat | This paper | 6b, 7c |
| | 24.96 | KGM-TSa190030a | 28660±210 | 33420-31920 | 32740±750 | Organic clay | This paper | 6b, 7c |
| | 30.85 | KGM-TSa190031 | 40130±450 | 44620-42980 | 43760±820 | Organic clay | This paper | 6b, 7c |
| **204 S4** | 5.8 | Beta analytic - 204 S4_5.8 | 1780±60 | 1830-1560 | 1690±130 | Peat | GMI, Sheet 204 | 6b |
| | 9.35 | Beta analytic - 204 S4_9.35 | 5280±50 | 6190-5930 | 6060±130 | Peat | GMI, Sheet 204 | 6b |
| | 21.0 | ENEA-204 S4_26.8 | 35500±3000 | 48350-35090 | 41030±6600 | Organic clay | GMI, Sheet 204 | 6b |
| **203 S9** | 11.45 | ENEA-203 S9_11.45 | 4350±80 | 5290-4810 | 4980±240 | Organic clay | GMI, Sheet 203 | 6b, 8a |
| | 20.25 | ENEA-203 S9_20.25 | 13450±320 | 17170-15270 | 16230±950 | Organic clay | GMI, Sheet 203 | 6b |
| **202 S1** | 11.40 | Beta analytic - 202 S1_11.4 | 9360±40 | 10700-10490 | 10600±100 | Organic clay | GMI, Sheet 202 | 6b |
| **202 S12** | 7.9 | Beta analytic - 202 S12_7.9 | 1480±80 | 1544-1275 | 1410±130 | Peat | GMI, Sheet 202 | 6b |
| | 15.0 | ENEA-202 S12_15.0 | 8020±90 | 9130-8600 | 8860±260 | Pedoge-nized clay | GMI, Sheet 202 | 6b |

| | | | | | | | | |
|---|---|---|---|---|---|---|---|---|
| **PP** | 31.30 | CIRCE – PP 31.3 | >45000 | - | - | Organic clay | Amorosi et al., 2017b | 6b |
| **SFP** | 11.7 | KGM-OWd160291 | 2480±40 | 2730-2370 | 2570±180 | Wood | This work | 6b |
| | 35.05 | CIRCE – DSH6715_H | 42400±800 | 47600-44370 | 45870±1600 | Pedoge-nized clay | This work | 6b |
| **Med** | 38.4 | CIRCE – Med_38.4 | >45000 | - | - | Organic clay | This work | 6b, 8b |
| **SP** | 9.60 | KGM-OSn160003 | 4360±40 | 5040-4840 | 4930±100 | Organic clay | This work | 6b |
| **Conc** | 13.6 | KGM-OSn160002 | 12230±70 | 14510-13900 | 14160±300 | Pedoge-nized clay | This work | 6b |
| **EM 19** | 10.5 | KGM-OWd160292 | 23080±140 | 27640-27120 | 27900±260 | Wood | This work | 6b |
| **Mn S1** | 18.8 | ENEA-Mn S1_18.8 | 38600±1050 | 44750-41270 | 42900±1700 | Organic clay | Amorosi et al., 2008 | 6b, 8c |
| | 27.7 | ENEA-Mn S1_27.7 | >45000 | - | - | Organic clay | Amorosi et al., 2008 | 6b, 8c |
| **239 S4** | 14.0 | ETH-239 S4_14 | 6255±75 | 7330-6950 | 7160±190 | Charcoal | GMI, Sheet 239 | 7a |
| | 28.0 | ETH-239 S4_28 | 12920±100 | 15770-15140 | 15450±310 | Peat | GMI, Sheet 239 | 7a |
| **239 S6** | 13.0 | Beta Analytic-239 S6_13 | 11840±150 | 14060-13390 | 13690±330 | Charcoal | GMI, Sheet 239 | 7a, 7c (Proj.222 S10) |
| **223 S11** | 6.25 | LODYC-223 S11_6.25 | 1235±40 | 1270-1060 | 1170±100 | Peat | GMI, Sheet 223 | 7b (Proj.) |
| **222 S2** | 7.0 | Beta Analytic-222 S2_7.0 | 340±60 | 510-290 | 390±110 | Peat | GMI, Sheet 222 | 7b |
| | 17.0 | Beta Analytic-222 S2_17.0 | 6000±60 | 6990-6670 | 6840±160 | Peat | GMI, Sheet 222 | 7b |
| | 20.9 | Beta Analytic-222 S2_20.9 | 7420±60 | 8380-8150 | 8250±110 | Organic clay | GMI, Sheet 222 | 7b |
| | 26.2 | Beta Analytic-222 S2_26.2 | 19770±150 | 24190-23420 | 23800±380 | Peat | GMI, Sheet 222 | 7b |
| **221 S1** | 16.35 | LODYC-221 S1_16.35 | 8945±200 | 10550-9540 | 10030±500 | Organic clay | GMI, Sheet 221 | 7b |
| | 29.8 | LODYC-221 S1_29.8 | 21780±800 | 27700-24410 | 26130±1600 | Organic clay | GMI, Sheet 221 | 7b |
| **EM 8** | 5.45 | OWd160064 | 4890±50 | 5740-5480 | 5630±130 | Peat | (Bruno et al., 2017) | 7c |
| | 7.30 | OWd160065 | 5800±400 | 6720-6490 | 6600±110 | Wood | (Bruno et al., 2017) | 7c |
| | 22.40 | OWd160066 | 7950±40 | 8890-8640 | 8820±120 | Wood | (Bruno et al., 2017) | 7c |
| **B3** | 3.55 | KGM-TWd190145 | 2120±20 | 2160-2000 | 2090±80 | Peat | This paper | 7c |
| | 8.5 | KGM-TWd190152 | 6480±30 | 7440-7310 | 7380±60 | Peat | This paper | 7c |
| | 9.2 | KGM-TSa190025 | 8870±50 | 10180-9760 | 10000±210 | Bulk sediment | This paper | 7c |
| | 12.6 | KGM-TSa190026 | 23750±140 | 28130-27580 | 27820±270 | Bulk sediment | This paper | 7c |
| | 15.6 | KGM-TSa190028 | 28590±200 | 33300-31840 | 32630±730 | Organic clay | This paper | 7c |

| | | | | | | | | |
|---|---|---|---|---|---|---|---|---|
| **204 S17** | 12.8 | KGM-OWd170597-1 | 3850±30 | 4410-4150 | 4270±130 | Plant frag. | This paper | 7c |
| | 17.0 | KGM-OWd170601-1 | 6840±30 | 7740-7600 | 7670±70 | Plant frag. | This paper | 7c |
| **B2** | 11.15 | KGM-TWd180570a | 650±30 | 610-550 | 610±30 | Wood | This paper | 7c |
| | 16.6 | KGM-TWd180575a | 2730±30 | 2880-2760 | 2820±60 | Wood | This paper | 7c |
| | 20.25 | KGM-TWd180577a | 5390±30 | 6290-6170 | 6210±60 | Wood | This paper | 7c |
| | 22.05 | KGM-TSa180035a | 9500±40 | 10870-10650 | 10840±100 | Bulk sediment | This paper | 7c |
| | 29.8 | KGM-TSa180036a | 246300±90 | 28900-28410 | 28660±240 | Bulk sediment | This paper | 7c |
| **222 S17** | 5.0 | LODYC-222 S17_5 | 2635±80 | 2950-2480 | 2730±230 | Organic clay | GMI, Sheet 222 | 7b (Proj.), 7c |
| **222 S6** | 3.9 | Beta Analytic-222 S6_3.9 | 2100±70 | 2210-1900 | 2090±150 | Organic clay | GMI, Sheet 222 | 7c |
| | 18.8 | Beta Analytic-222 S6_18.8 | 11560±60 | 13500-13270 | 13390±110 | Organic clay | GMI, Sheet 222 | 7b (Proj.), 7c |
| | 26.8 | Beta Analytic-222 S6_26.8 | 18000±150 | 22260-21400 | 21810±430 | Peat | GMI, Sheet 222 | 7b (Proj.), 7c |
| **222 S10** | 12.5 | Beta Analytic-222 S10_12.5 | 14280±140 | 17800-16980 | 17380±410 | Organic clay | GMI, Sheet 222 | 7c |
| | 21.2 | Beta Analytic-222 S10_21.2 | 32550±600 | 36770-35350 | 36770±700 | Peat | GMI, Sheet 222 | 7c |
| | 35.5 | Beta Analytic-222 S10_35.5 | >44500 | - | - | Wood | GMI, Sheet 222 | 7c |
| **221 S5** | 24.0 | LODYC – 221 S5_24 | 19760±900 | 26010-21930 | 23970±2000 | Organic clay | GMI, Sheet 221 | 8a |
| **221 S3** | 15.20 | LODYC – 221 S3_15.2 | 13025±160 | 16070-15150 | 15610±460 | Organic clay | GMI, Sheet 221 | 8a |
| | 22.80 | LODYC – 221 S3_22.8 | >35000 | - | - | Organic clay | GMI, Sheet 221 | 8a |
| **CS** | 23.05 | ETH-50655 | 26917±89 | 31190-30820 | 31010±180 | Shell | This work | 8b (Proj.) |
| **201 S6** | 17.6 | ENEA-201 S6_17.6 | 4530±60 | 5330-4970 | 5170±180 | - | GMI, Sheet 201 | 8b |
| | 33.9 | ENEA-201 S6_33.9 | 26500±200 | 31080-30370 | 30750±350 | - | GMI, Sheet 201 | 8b |
| **201 S4** | 9.9 | ENEA-201 S4_9.9 | 7780±110 | 8810-8380 | 8620±210 | - | GMI, Sheet 201 | 8b |
| | 15.7 | ENEA-201 S4_15.7 | 12200±180 | 14990-13710 | 14240±640 | - | GMI, Sheet 201 | 8b |
| | 21.4 | ENEA-201 S4_21.4 | 19340±200 | 23840-22800 | 23300±520 | - | GMI, Sheet 201 | 8b |
| | 24.1 | ENEA-201 S4_24.1 | 21250±350 | 26190-24600 | 25510±800 | - | GMI, Sheet 201 | 8b |
| **201 S3** | 17.15 | ENEA-201 S3_17.15 | 6890±80 | 7870-7580 | 7740±140 | - | GMI, Sheet 201 | 8b |
| | 28.7 | ENEA-201 S3_28.7 | 14000±100 | 17360-16620 | 16990±370 | - | GMI, Sheet 201 | 8b |
| **182 S10** | 6.4 | ENEA-182 S10_6.4 | 2890±50 | 3170-2870 | 3030±150 | Organic clay | GMI, Sheet 182 | 8c |
| | 30.5 | ENEA-182 S10_30.5 | 47900±550 | 49090-46860 | 47960±1100 | Organic clay | GMI, Sheet 182 | 8c |
| **182 S15** | 10.3 | ENEA-182 S15_10.5 | 4930±80 | 5895-5485 | 5680±200 | Organic clay | (Pavesi, 2009) | 8c |

| | | | | | | | | |
|---|---|---|---|---|---|---|---|---|
| | 19.5 | ENEA-182 S15_19.5 | 15450±130 | 18967-18429 | 18715±270 | Wood | Pavesi, 2009 | 8c |
| | 34.7 | ENEA-182 S15_34.7 | 27300±600 | 32961-30371 | 31380±1300 | Wood | Pavesi, 2009 | 8c |
| | 45.0 | ENEA-182 S15_45.0 | >45000 | - | - | Organic clay | Pavesi, 2009 | 8c |
| **182 S3** | 3.65 | ENEA-182 S3_3.65 | 1830±60 | 1900-1600 | 1760±150 | Soil | GMI, Sheet 182 | 8c |
| | 14.1 | ENEA-182 S3_14.1 | 15750±110 | 19310-18760 | 19020±270 | Soil | GMI, Sheet 182 | 8c |
| | 18.4 | ENEA-182 S3_18.4 | 17850±150 | 22020-21140 | 21610±440 | Soil | GMI, Sheet 182 | 8c |

## References


Aitken, M.J., 1985. Thermoluminescence dating. Academic Press, London.

Amadori, C., Toscani, G., Di Giulio, A., Maesano, F.E., D'Ambrogi, C., Ghielmi, M., Fantoni, R., 2019. From cylindrical to non-cylindrical foreland basin: Pliocene–Pleistocene evolution of the Po Plain–Northern Adriatic basin (Italy). Basin Res. 991–1015. https://doi.org/10.1111/bre.12369

Amorosi, A., Antonioli, F., Bertini, A., Marabini, S., Mastronuzzi, G., Montagna, P., Negri, A., Rossi, V., Scarponi, D., Taviani, M., Angeletti, L., Piva, A., Vai, G.B., 2014. The Middle-Upper Pleistocene Fronte Section (Taranto, Italy): An exceptionally preserved marine record of the Last Interglacial. Glob. Planet. Change 119, 23–38. https://doi.org/10.1016/j.gloplacha.2014.04.007

Amorosi, A., Bruno, L., Campo, B., Costagli, B., Dinelli, E., Hong, W., Sammartino, I., Vaiani, S.C., 2019. Tracing clinothem geometry and sediment pathways in the prograding Holocene Po Delta system through integrated core stratigraphy. Basin Res. 1–10. https://doi.org/10.1111/bre.12360

Amorosi, A., Bruno, L., Campo, B., Morelli, A., 2015. The value of pocket penetration tests for the high-resolution palaeosol stratigraphy of late Quaternary deposits. Geol. J. 50, 670–682.

Amorosi, A., Bruno, L., Campo, B., Morelli, A., Rossi, V., Scarponi, D., Hong, W., Bohacs, K.M., Drexler, T.M., 2017a. Global sea-level control on local parasequence architecture from the Holocene record of the Po Plain, Italy. Mar. Pet. Geol. 87, 99–111. https://doi.org/10.1016/j.marpetgeo.2017.01.020

Amorosi, A., Bruno, L., Cleveland, D.M., Morelli, A., Hong, W., 2017b. Paleosols and associated channel-belt sand bodies from a continuously subsiding late quaternary system (Po basin, Italy): New insights into continental sequence stratigraphy. Bull. Geol. Soc. Am. 129, 449–463. https://doi.org/10.1130/B31575.1

645 Amorosi, A., Centineo, M.C., Colalongo, M.L., Pasini, G., Sarti, G., Vaiani, S.C., 2003. Facies architecture
646 and latest Pleistocene–Holocene depositional history of the Po Delta (Comacchio area), Italy. J. Geol.
647 111, 39–56.
648 Amorosi, A., Colalongo, M.L., 2005. The linkage between alluvial and coeval nearshore marine successions:
649 evidence from the Late Quaternary record of the Po River Plain, Italy. Fluv. Sedimentol. VII 255–275.
650 Amorosi, A., Colalongo, M.L., Fiorini, F., Fusco, F., Pasini, G., Vaiani, S.C., Sarti, G., 2004.
651 Palaeogeographic and palaeoclimatic evolution of the Po Plain from 150-ky core records. Glob. Planet.
652 Change 40, 55–78. https://doi.org/10.1016/S0921-8181(03)00098-5
653 Amorosi, A., Colalongo, M.L., Fusco, F., Pasini, G., Fiorini, F., 1999a. Glacio-eustatic control of
654 continental-shallow marine cyclicity from late quaternary deposits of the southeastern Po Plain,
655 northern Italy. Quat. Res. 52, 1–13. https://doi.org/10.1006/qres.1999.2049
656 Amorosi, A, Colalongo, M., Pasini, G., Preti, D., 1999b. Sedimentary response to Late Quaternary sea-level
657 changes in the Romagna coastal plain(northern Italy). Sedimentology 46, 99–121.
658 Amorosi, A., Forlani, L., Fusco, F., Severi, P., 2001. Cyclic patterns of facies and pollen associations from
659 late quaternary deposits in the subsurface of Bologna. GeoActa 1, 83–94.
660 Amorosi, A., Marchi, N., 1999. High-resolution sequence stratigraphy from piezocone tests: An example
661 from the Late Quaternary deposits of the southeastern Po Plain. Sediment. Geol. 128, 67–81.
662 https://doi.org/10.1016/S0037-0738(99)00062-7
663 Amorosi, A., Pavesi, M., Ricci Lucchi, M., Sarti, G., Piccin, A., 2008. Climatic signature of cyclic fluvial
664 architecture from the Quaternary of the central Po Plain, Italy. Sediment. Geol. 209, 58–68.
665 https://doi.org/10.1016/j.sedgeo.2008.06.010
666 Antonioli, F., 2012. Sea level change in Western-Central Mediterranean since 300 kyr: Comparing global sea
667 level curves with observed data. Alp. Mediterr. Quat. 25, 15–23.
668 Antonioli, F., Anzidei, M., Amorosi, A., Lo Presti, V., Mastronuzzi, G., Deiana, G., De Falco, G., Fontana,
669 A., Fontolan, G., Lisco, S., Marsico, A., Moretti, M., Orrù, P.E., Sannino, G.M., Serpelloni, E.,
670 Vecchio, A., 2017. Sea-level rise and potential drowning of the Italian coastal plains: Flooding risk
671 scenarios for 2100. Quat. Sci. Rev. 158, 29–43. https://doi.org/10.1016/j.quascirev.2016.12.021
672 Antonioli, F., Bard, E., Potter, E.K., Silenzi, S., Improta, S., 2004. 215-ka history of sea-level oscillations

673 from marine and continental layers in Argentarola Cave speleothems (Italy). Glob. Planet. Change 43,
674 57–78. https://doi.org/10.1016/j.gloplacha.2004.02.004
675 Banerjee, D., Murray, A.S., Bøtter-Jensen, L., Lang, A., 2001. Equivalent dose estimation using a single
676 aliquot of polymineral fine grains. Radiat. Meas. 33, 73–94.
677 Bard, E., Antonioli, F., Silenzi, S., 2002. Sea-level during the penultimate interglacial period based on a
678 submerged stalagmite from Argentarola Cave (Italy). Earth Planet. Sci. Lett. 196, 135–146.
679 https://doi.org/10.1016/S0012-821X(01)00600-8
680 Bard, E., Hamelin, B., Fairbanks, R.G., 1990. U-Th ages obtained by mass spectrometry in corals from
681 Barbados: Sea level during the past 130,000 years. Nature 346, 456–458.
682 https://doi.org/10.1038/346456a0
683 Bardají, T., Goy, J.L., Zazo, C., Hillaire-Marcel, C., Dabrio, C.J., Cabero, A., Ghaleb, B., Silva, P.G., Lario,
684 J., 2009. Sea level and climate changes during OIS 5e in the Western Mediterranean. Geomorphology
685 104, 22–37. https://doi.org/10.1016/j.geomorph.2008.05.027
686 Basili, R., Barba, S., 2007. Migration and shortening rates in the northern Apennines, Italy: Implications for
687 seismic hazard. Terra Nov. 19, 462–468. https://doi.org/10.1111/j.1365-3121.2007.00772.x
688 Blum, M.D., Martin, J., Milliken, K., Garvin, M., 2013. Paleovalley systems: Insights from Quaternary
689 analogs and experiments. Earth-Science Rev. 116, 128–169.
690 https://doi.org/10.1016/j.earscirev.2012.09.003
691 Blum, M.D., Aslan, A., 2006. Signatures of climate vs. sea-level change within incised valley-fill
692 successions: Quaternary examples from the Texas GULF Coast. Sediment. Geol. 190, 177–211.
693 https://doi.org/10.1016/j.sedgeo.2006.05.024
694 Blum, M.D., Törnqvist, T.E., 2000. Fluvial responses to climate and sea-level change: A review and look
695 forward. Sedimentology 47, 2–48. https://doi.org/10.1046/j.1365-3091.2000.00008.x
696 Boccaletti, M., Corti, G., Martelli, L., 2011. Recent and active tectonics of the external zone of the Northern
697 Apennines (Italy). Int. J. Earth Sci. 100, 1331–1348. https://doi.org/10.1007/s00531-010-0545-y
698 Bondesan, M., Cibin, U., Colalongo, M., Pugliese, N., Stefani, M., Tsakiridis, E., Vaiani, S.C., Vincenzi, S.,
699 2006. Benthic communities and sedimentary facies recording late Quaternary environmental
700 fluctuations in a Po Delta subsurface succession (Northern Italy), in: 2nd and 3rd Italian Meeting on

701 Environmental Micropaleontology. Grzybowski Founfation Special Publication, pp. 21–31.
702 Bordoni, P., Valensise, G., 1998. Deformation of the 125 ka marine terrace in Italy: tectonic implications.
703 Geol. Soc. Spec. Publ. 146, 71–110. https://doi.org/10.1144/GSL.SP.1999.146.01.05
704 Bøtter-Jensen, L., 1997. Luminescence techniques: instrumentation and methods. Radiat. Meas. 27, 749–
705 768.
706 Bøtter-Jensen, L., 1988. The automated Risø TL dating reader system. Int. J. Radiat. Appl. Instrumentation.
707 Part D. Nucl. Tracks Radiat. Meas. 14, 177–180.
708 Bøtter-Jensen, L., Bulur, E., Duller, G.A.T., Murray, A.S., 2000. Advances in luminescence instrument
709 systems. Radiat. Meas. 32, 523–528.
710 Bruno, L., Bohacs, K.M., Campo, B., Drexler, T.M., Rossi, V., Sammartino, I., Scarponi, D., Hong, W.,
711 Amorosi, A., 2017. Early Holocene transgressive palaeogeography in the Po coastal plain (northern
712 Italy). Sedimentology 64, 1792–1816. https://doi.org/10.1111/sed.12374
713 Burrato, P., Ciucci, F., Valensise, G., 2003. An inventory of river anomalies in the Po Plain, Northern Italy:
714 Evidence for active blind thrust faulting. Ann. Geophys. 46, 865–882. https://doi.org/10.4401/ag-3459
715 Busschers, F.S., Kasse, C., van Balen, R.T., Vandenberghe, J., Cohen, K.M., Weerts, H.J.T., Wallinga, J.,
716 Johns, C., Cleveringa, P., Bunnik, F.P.M., 2007. Late Pleistocene evolution of the Rhine-Meuse system
717 in the southern North Sea basin: imprints of climate change, sea-level oscillation and glacio-isostacy.
718 Quat. Sci. Rev. 26, 3216–3248. https://doi.org/10.1016/j.quascirev.2007.07.013
719 Busschers, F.S., Weerts, H.J.T., Wallinga, J., Cleveringa, P., Kasse, C., de Wolf, H., Cohen, K.M., 2005.
720 Sedimentary architecture and optical dating of Middle and Late Pleistocene Rhine-Meuse deposits -
721 Fluvial response to climate change, sea-level fluctuation and glaciation. Geol. en
722 Mijnbouw/Netherlands J. Geosci. 84, 25–41. https://doi.org/10.1017/s0016774600022885
723 Campo, B., Amorosi, A., Bohacs, K.M., in press. Late Quaternary sequence stratigraphy as a tool for
724 groundwater exploration: lessons from the Po River Basin (northern Italy). Am. Assoc. Pet. Geol. Bull.
725 https://doi.org/10.1306/06121918116
726 Campo, B., Amorosi, A., Bruno, L., 2016. Contrasting alluvial architecture of Late Pleistocene and Holocene
727 deposits along a 120-km transect from the central Po Plain (northern Italy). Sediment. Geol. 341, 265–
728 275.

729 Campo, B., Amorosi, A., Vaiani, S.C., 2017. Sequence stratigraphy and late Quaternary paleoenvironmental
730 evolution of the Northern Adriatic coastal plain (Italy). Palaeogeogr. Palaeoclimatol. Palaeoecol. 466,
731 265–278. https://doi.org/10.1016/j.palaeo.2016.11.016
732 Caputo, R., Pellegrinelli, A., Bignami, C., Bondesan, A., Mantovani, A., Stramondo, S., Russo, P., 2015.
733 High-precision levelling, DInSAR and geomorphological effects in the Emilia 2012 epicentral area.
734 Geomorphology 235, 106–117. https://doi.org/10.1016/j.geomorph.2015.02.002
735 Carboni, M.G., Bergamin, L., Di Bella, L., Esu, D., Cerone, E.P., Antonioli, F., Verrubbi, V., 2010.
736 Palaeoenvironmental reconstruction of late Quaternary foraminifera and molluscs from the ENEA
737 borehole (Versilian plain, Tuscany, Italy). Quat. Res. 74, 265–276.
738 https://doi.org/10.1016/j.yqres.2010.07.006
739 Carminati, E., Di Donato, G., 1999. Separating natural and anthropogenic vertical movements in fast
740 subsiding areas: The Po plain (N. Italy) case. Geophys. Res. Lett. 26, 2291–2294.
741 https://doi.org/10.1029/1999GL900518
742 Carminati, E., Doglioni, C., 2012. Alps vs. Apennines: The paradigm of a tectonically asymmetric Earth.
743 Earth-Science Rev. 112, 67–96. https://doi.org/10.1016/j.earscirev.2012.02.004
744 Carminati, E., Doglioni, C., Scrocca, D., 2003. Apennines subduction-related subsidence of Venice (Italy).
745 Geophys. Res. Lett. 30, 1–4. https://doi.org/10.1029/2003GL017001
746 Carr, A.S., Bateman, M.D., Roberts, D.L., Murray-Wallace, C. V., Jacobs, Z., Holmes, P.J., 2010. The last
747 interglacial sea-level high stand on the southern Cape coastline of South Afri~ Quat. Res. 73, 351–363.
748 https://doi.org/10.1016/j.yqres.2009.08.006
749 Castorina, F., Vaiani, S.C., 2018. Riverine influence in Sr isotope ratio of mollusk shells and relationship
750 with foraminiferal assemblages in a late Quaternary succession of the Po River Delta (northern Italy).
751 Ital. J. Geosci. 137, 31–37. https://doi.org/10.3301/IJG.2017.15
752 Chappell, J., Omura, A., Esat, T., McCulloch, M., Pandolfi, J., Ota, Y., Pillans, B., 1996. Reconciliation of
753 late Quaternary sea levels derived from coral terraces at Huon Peninsula with deep sea oxygen isotope
754 records. Earth Planet. Sci. Lett. 141, 227–236. https://doi.org/10.1016/0012-821x(96)00062-3
755 Chappell, J., Shackleton, N., 1986. Oxygen isotopes and sea level. Nature 324, 137–140.
756 Church, J.A., Clark, P.U., Cazenave, A., Gregory, J.M., Jevrejeva, S., Levermann, A., Merrifield, M.A.,

Milne, G.A., Nerem, R.S., Nunn, P.D., 2013. Sea level change. PM Cambridge University Press.

Clark, P.U., Huybers, P., 2009. Global change: Interglacial and future sea level. Nature 462, 856–857. https://doi.org/10.1038/462856a

Creveling, J.R., Mitrovica, J.X., Hay, C.C., Austermann, J., Kopp, R.E., 2015. Revisiting tectonic corrections applied to Pleistocene sea-level highstands. Quat. Sci. Rev. 111, 72–80. https://doi.org/10.1016/j.quascirev.2015.01.003

De Santis, V., Caldara, M., de Torres, T., Ortiz, J.E., 2010. Stratigraphic units of the Apulian Tavoliere plain (Southern Italy): Chronology, correlation with marine isotope stages and implications regarding vertical movements. Sediment. Geol. 228, 255–270. https://doi.org/10.1016/j.sedgeo.2010.05.001

Durcan, J.A., King, G.E., Duller, G.A.T., 2015. DRAC: Dose Rate and Age Calculator for trapped charge dating. Quat. Geochronol. 28, 54–61.

Dutton, A., Carlson, A.E., Long, Aj., Milne, G.A., Clark, P.U., DeConto, R., Horton, B.P., Rahmstorf, S., Raymo, M.E., 2015. Sea-level rise due to polar ice-sheet mass loss during past warm periods. Science (80-. ). 349, aaa4019.

Dutton, A., Lambeck, K., 2012. Ice volume and sea level during the last interglacial. Science (80-. ). 337, 216–219. https://doi.org/10.1126/science.1205749

Ferranti, L., Antonioli, F., Anzidei, M., Monaco, C., Stocchi, P., 2010. The timescale and spatial extent of vertical tectonic motions in Italy: Insights from coastal tectonic studies. Rend. Online Soc. Geol. Ital. 11, 683–684. https://doi.org/10.3809/jvirtex.2009.00255

Ferranti, L., Antonioli, F., Mauz, B., Amorosi, A., Dai Pra, G., Mastronuzzi, G., Monaco, C., Orrù, P., Pappalardo, M., Radtke, U., Renda, P., Romano, P., Sansò, P., Verrubbi, V., 2006. Markers of the last interglacial sea-level high stand along the coast of Italy: Tectonic implications. Quat. Int. 145–146, 30–54. https://doi.org/10.1016/j.quaint.2005.07.009

Fiorini, F., 2004. Benthic foraminiferal associations from Upper Quaternary deposits of southeastern Po Plain, Italy. Micropaleontology 50, 45–58. https://doi.org/10.2113/50.1.45

Fontana, A., Mozzi, P., Bondesan, A., 2010. Late Pleistocene evolution of the Venetian-Friulian Plain. Rend. Lincei 21, 181–196. https://doi.org/10.1007/s12210-010-0093-1

Fontana, A., Mozzi, P., Marchetti, M., 2014. Alluvial fans and megafans along the southern side of the Alps.

785 Sediment. Geol. 301, 150–171. https://doi.org/10.1016/j.sedgeo.2013.09.003
786 Galili, E., Zviely, D., Ronen, A., Mienis, H.K., 2007. Beach deposits of MIS 5e high sea stand as indicators
787 for tectonic stability of the Carmel coastal plain, Israel. Quat. Sci. Rev. 26, 2544–2557.
788 https://doi.org/10.1016/j.quascirev.2007.06.027
789 Ghielmi, M., Minervini, M., Nini, C., Rogledi, S., Rossi, M., 2013. Late Miocene-Middle Pleistocene
790 sequences in the Po Plain - Northern Adriatic Sea (Italy): The stratigraphic record of modification
791 phases affecting a complex foreland basin. Mar. Pet. Geol. 42, 50–81.
792 https://doi.org/10.1016/j.marpetgeo.2012.11.007
793 Guérin, G., Mercier, N., Adamiec, G., 2011. Dose-rate conversion factors: update. Anc. TL 29, 5–8.
794 Guillaume, M.M.M., Reyss, J.L., Pirazzoli, P.A., Bruggemann, J.H., 2013. Tectonic stability since the last
795 interglacial offsets the Glorieuses Islands from the nearby Comoros archipelago. Coral Reefs 32, 719–
796 726. https://doi.org/10.1007/s00338-012-1006-9
797 Hori, K., Saito, Y., Zhao, Q., Wang, P., 2002. Evolution of the coastal depositional systems of the
798 Changjiang (Yangtze) River in response to Late Pleistocene-Holocene sea-level changes. J. Sediment.
799 Res. 72, 884–897. https://doi.org/10.1306/052002720884
800 Horton, B.P., Kopp, R.E., Dutton, A., Shaw, T.A., Carolina, N., 2019. Geological records of past sea-level
801 changes as constraints for future projections. Past Glob. Chang. Mag. 27, 28–29.
802 https://doi.org/10.22498/pages.27.1.28
803 Intergovernmental Panel on Climate Change, 2018. Global Warming of 1.5° C: An IPCC Special Report on
804 the Impacts of Global Warming of 1.5° C Above Pre-industrial Levels and Related Global Greenhouse
805 Gas Emission Pathways, in the Context of Strengthening the Global Response to the Threat of Climate
806 Chang. Intergovernmental Panel on Climate Change.
807 Intergovernmental Panel on Climate Change, 2007. The physical science basis. Contrib. Work. Gr. I to
808 fourth Assess. Rep. Intergov. Panel Clim. Chang. 996.
809 Kopp, R.E., Simons, F.J., Mitrovica, J.X., Maloof, A.C., Oppenheimer, M., 2009. Probabilistic assessment of
810 sea level during the last interglacial stage. Nature 462, 863–867. https://doi.org/10.1038/nature08686
811 Kukla, G.J., Bender, M.L., de Beaulieu, J.-L., Bond, G., Broecker, W.S., Cleveringa, P., Gavin, J.E., Herbert,
812 T.D., Imbrie, J., Jouzel, J., 2002. Last interglacial climates. Quat. Res. 58, 2–13.

https://doi.org/10.4135/9781446247501.n2234

Lambeck, K., Antonioli, F., Purcell, A., Silenzi, S., 2004. Sea-level change along the Italian coast for the past 10,000 yr. Quat. Sci. Rev. 23, 1567–1598. https://doi.org/10.1016/j.quascirev.2004.02.009

Maesano, F.E., D'Ambrogi, C., Burrato, P., Toscani, G., 2015. Slip-rates of blind thrusts in slow deforming areas: Examples from the Po Plain (Italy). Tectonophysics 643, 8–25. https://doi.org/10.1016/j.tecto.2014.12.007

Malinverno, A., Ryan, W.B.F., 1986. BBBn 5, 227–245.

Mariotti, G., Doglioni, C., 2000. The dip of the foreland monocline in the Alps and Apennines. Earth Planet. Sci. Lett. 181, 191–202. https://doi.org/10.1016/S0012-821X(00)00192-8

Martinson, D.G., Pisias, N.G., Hays, J.D., Imbrie, J., Moore, T.C., Shackleton, N.J., 1987. Age dating and the orbital theory of the ice ages: Development of a high-resolution 0 to 300,000-year chronostratigraphy. Quat. Res. 27, 1–29. https://doi.org/10.1016/0033-5894(87)90046-9

Matsu'ura, T., Komatsubara, J., Wu, C., 2019. Accurate determination of the Pleistocene uplift rate of the NE Japan forearc from the buried MIS 5e marine terrace shoreline angle. Quat. Sci. Rev. 212, 45–68. https://doi.org/10.1016/j.quascirev.2019.03.007

Mauz, B., Fanelli, F., Elmejdoub, N., Barbieri, R., 2012. Coastal response to climate change: Mediterranean shorelines during the Last Interglacial (MIS 5). Quat. Sci. Rev. 54, 89–98. https://doi.org/10.1016/j.quascirev.2012.02.021

Milli, S., D'Ambrogi, C., Bellotti, P., Calderoni, G., Carboni, M.G., Celant, A., Di Bella, L., Di Rita, F., Frezza, V., Magri, D., Pichezzi, R.M., Ricci, V., 2013. The transition from wave-dominated estuary to wave-dominated delta: The Late Quaternary stratigraphic architecture of Tiber River deltaic succession (Italy). Sediment. Geol. 284–285, 159–180. https://doi.org/10.1016/j.sedgeo.2012.12.003

Milli, S., Mancini, M., Moscatelli, M., Stigliano, F., Marini, M., Cavinato, G.P., 2016. From river to shelf, anatomy of a high-frequency depositional sequence: The Late Pleistocene to Holocene Tiber depositional sequence. Sedimentology 63, 1886–1928. https://doi.org/10.1111/sed.12277

Murray-Wallace, C. V., 2013. Eustatic Sea-Level Changes - Glacial-Interglacial Cycles, 2nd ed, Encyclopedia of Quaternary Science: Second Edition. Elsevier B.V. https://doi.org/10.1016/B978-0-444-53643-3.00132-1

841 Murray-Wallace, C. V., 2002. Pleistocene coastal stratigraphy, sea-level highstands and neotectonism of the
842 southern Australian passive continental margin - A review. J. Quat. Sci. 17, 469–489.
843 https://doi.org/10.1002/jqs.717
844 Murray-Wallace, C. V., Belperio, A.P., Dosseto, A., Nicholas, W.A., Mitchell, C., Bourman, R.P., Eggins,
845 S.M., Grün, R., 2016. Last interglacial (MIS 5e) sea-level determined from a tectonically stable, far-
846 field location, Eyre Peninsula, southern Australia. Aust. J. Earth Sci. 63, 611–630.
847 https://doi.org/10.1080/08120099.2016.1229693
848 Murray-Wallace, C. V, Woodroffe, C.D., 2014. Quaternary sea-level changes: a global perspective.
849 Cambridge University Press.
850 Murray, A.S., Wintle, A.G., 2000. Luminescence dating of quartz using an improved single-aliquot
851 regenerative-dose protocol. Radiat. Meas. 32, 57–73.
852 Muttoni, G., Carcano, C., Garzanti, E., Ghielmi, M., Piccin, A., Pini, R., Rogledi, S., Sciunnach, D., 2003.
853 Onset of major Pleistocene glaciations in the Alps. Geology 31, 989–992.
854 https://doi.org/10.1130/G19445.1
855 Nakazawa, T., Sakata, K., Hongo, M., Nakazato, H., 2017. Transition from incised valley to barrier island
856 systems during MIS 5e in the northern Chiba area, Kanto Plain, central Japan. Quat. Int. 456, 85–101.
857 https://doi.org/10.1016/j.quaint.2017.06.031
858 Oliver, T.S.N., Kennedy, D.M., Tamura, T., Murray-Wallace, C. V., Konlechner, T.M., Augustinus, P.C.,
859 Woodroffe, C.D., 2018. Interglacial-glacial climatic signatures preserved in a regressive coastal barrier,
860 southeastern Australia. Palaeogeogr. Palaeoclimatol. Palaeoecol. 501, 124–135.
861 https://doi.org/10.1016/j.palaeo.2018.04.011
862 Ori, G.G., 1993. Continental depositional systems of the Quaternary of the Po Plain (northern Italy).
863 Sediment. Geol. 83, 1–14.
864 Ori, G.G., Friend, P.F., 1984. Sedimentary basins formed and carried piggyback on active thrust sheets.
865 Geology 12, 475–478. https://doi.org/10.1130/0091-7613(1984)12<475:SBFACP>2.0.CO;2
866 Otvos, E.G., 2015. The Last Interglacial Stage: Definitions and marine highstand, North America and
867 Eurasia. Quat. Int. 383, 158–173. https://doi.org/10.1016/j.quaint.2014.05.010
868 Otvos, E.G., 2013. Rapid and widespread response of the Lower Mississippi River to eustatic forcing during

the last glacial-interglacial cycle: Discussion. Bull. Geol. Soc. Am. 125, 1369–1374.

Otvos, E.G., 2005. Numerical chronology of Pleistocene coastal plain and valley development; extensive aggradation during glacial low sea-levels. Quat. Int. 135, 91–113. https://doi.org/10.1016/j.quaint.2004.10.026

Overpeck, J.T., Otto-bliesner, B.L., Miller, G.H., Daniel, R., Alley, R.B., Kiehl, J.T., Overpeck, J.T., Otto-bliesner, B.L., Miller, G.H., Muhs, D.R., Alley, R.B., Kiehl, J.T., 2006. Paleoclimatic evidence for future ice-sheet instability and rapid sea-level rise. *Science*, *311*(5768), 1747-1750.

Pavesi, M., 2009. Architettura stratigrafica dei depositi medio-e tardoquaternari del bacino padano, finalizzata alla caratterizzazione geometrica degli acquiferi.

Peeters, J., Busschers, F.S., Stouthamer, E., 2015. Fluvial evolution of the Rhine during the last interglacial-glacial cycle in the southern North Sea basin: A review and look forward. Quat. Int. 357, 176–188. https://doi.org/10.1016/j.quaint.2014.03.024

Peeters, J., Busschers, F.S., Stouthamer, E., Bosch, J.H.A., Van den Berg, M.W., Wallinga, J., Versendaal, A.J., Bunnik, F.P.M., Middelkoop, H., 2016. Sedimentary architecture and chronostratigraphy of a late Quaternary incised-valley fill: A case study of the late Middle and Late Pleistocene Rhine system in the Netherlands. Quat. Sci. Rev. 131, 211–236. https://doi.org/10.1016/j.quascirev.2015.10.015

Peeters, J., Cohen, K.M., Thrana, C., Busschers, F.S., Martinius, A.W., Stouthamer, E., Middelkoop, H., 2019. Preservation of Last Interglacial and Holocene transgressive systems tracts in the Netherlands and its applicability as a North Sea Basin reservoir analogue. Earth-Science Rev. 188, 482–497. https://doi.org/10.1016/j.earscirev.2018.10.010

Picotti, V., Pazzaglia, F.J., 2008. A new active tectonic model for the construction of the Northern Apennines mountain front near Bologna (Italy). J. Geophys. Res. Solid Earth 113, 1–24. https://doi.org/10.1029/2007JB005307

Pieri, M., Groppi, G., 1981. Subsurface geological structure of the Po Plain, Italy. Verlag nicht ermittelbar.

Pirazzoli, P.A., 1993. Global sea-level changes and their measurement. Glob. Planet. Change 8, 135–148. https://doi.org/10.1016/0921-8181(93)90021-F

Pondrelli, S., Salimbeni, S., Perfetti, P., Danecek, P., 2012. Quick regional centroid moment tensor solutions for the Emilia 2012 (northern Italy) seismic sequence. Ann. Geophys. 55, 615–621.

https://doi.org/10.4401/ag-6146

Prescott, J.R., Hutton, J.T., 1994. Cosmic ray contributions to dose rates for luminescence and ESR dating: large depths and long-term time variations. Radiat. Meas. 23, 497–500.

Ramsey, C.B., Lee, S., 2013. Recent and Planned Developments of the Program OxCal. Radiocarbon 55, 720–730. https://doi.org/10.1017/s0033822200057878

Regione Emilia-Romagna and Eni-Agip, 1998. Riserve idriche sotterranee della Regione Emilia-Romagna. Ed. by G. Di Dio, Publ. by Publ. by SELCA, Firenze 120.

Regione Lombardia and Eni Divisione Agip, 2002. Geologia degli acquiferi padani della Regione Lombardia. SELCA, Firenze.

Reimer, P.J., Edouard Bard, B., Alex Bayliss, B., Warren Beck, B.J., Paul Blackwell, B.G., Christopher Bronk Ramsey, B., 2013. Intcal13 and Marine13 Radiocarbon Age Calibration Curves 0–50,000 Years Cal Bp. Radiocarbon 55, 1869–1887. https://doi.org/10.1017/S0033822200048864

Ricci Lucchi, F., Colalongo, M.L., Cremonini, G., Gasperi, G., Iaccarino, S., Papani, G., Raffi, S., Rio, D., 1982. Evoluzione sedimentaria e paleogeografica nel margine appenninico. Guid. alla Geol. del margine appenninico-padano. Soc. Geol. It 17–46.

Richter, D., Richter, A., Dornich, K., 2015. Lexsyg smart—a luminescence detection system for dosimetry, material research and dating application. Geochronometria 42.

Rohling, E.J., Grant, K., Hemleben, C., Siddall, M., Hoogakker, B.A.A., Bolshaw, M., Kucera, M., 2008. High rates of sea-level rise during the last interglacial period. Nat. Geosci. 1, 38–42. https://doi.org/10.1038/ngeo.2007.28

Rossi, M., Minervini, M., Ghielmi, M., Rogledi, S., 2015. Messinian and Pliocene erosional surfaces in the Po Plain-Adriatic Basin: Insights from allostratigraphy and sequence stratigraphy in assessing play concepts related to accommodation and gateway turnarounds in tectonically active margins. Mar. Pet. Geol. 66, 192–216. https://doi.org/10.1016/j.marpetgeo.2014.12.012

Rovere, A., Raymo, M.E., Vacchi, M., Lorscheid, T., Stocchi, P., Gómez-Pujol, L., Harris, D.L., Casella, E., O'Leary, M.J., Hearty, P.J., 2016. The analysis of Last Interglacial (MIS 5e) relative sea-level indicators: Reconstructing sea-level in a warmer world. Earth-Science Rev. 159, 404–427. https://doi.org/10.1016/j.earscirev.2016.06.006

925 Royden, L., Patacca, E., Scandone, P., 1987. Segmentation and configuration of subducted lithosphere in
926 Italy: an important control on thrust-belt and foredeep-basin evolution. Geology 15, 714–717.
927 https://doi.org/10.1130/0091-7613(1987)15<714:SACOSL>2.0.CO;2
928 Sánchez Goñi, M.F., Bakker, P., Desprat, S., Carlson, A.E., Van Meerbeeck, C.J., Peyron, O., Naughton, F.,
929 Fletcher, W.J., Eynaud, F., Rossignol, L., Renssen, H., 2012. European climate optimum and enhanced
930 Greenland melt during the last interglacial. Geology 40, 627–630. https://doi.org/10.1130/G32908.1
931 Sánchez Goñi, M.F., Eynaud, F., Turon, J.L., Shackleton, N.J., 1999. High resolution palynological record
932 off the Iberian margin: Direct land-sea correlation for the Last Interglacial complex. Earth Planet. Sci.
933 Lett. 171, 123–137. https://doi.org/10.1016/S0012-821X(99)00141-7
934 Scarponi, D., Kaufman, D., Amorosi, A., Kowalewski, M., 2013. Sequence stratigraphy and the resolution of
935 the fossil record. Geology 41, 239–242.
936 Scarponi, D., Kowalewski, M., 2004. Stratigraphic paleoecology: Bathymetric signatures and sequence
937 overprint of mollusk associations from upper Quaternary sequences of the Po Plain, Italy. Geology 32,
938 989–992. https://doi.org/10.1130/G20808.1
939 Scrocca, D., Carminati, E., Doglioni, C., Marcantoni, D., 2007. Slab retreat and active shortening along the
940 central-northern Apennines, in: Thrust Belts and Foreland Basins. Springer, pp. 471–487.
941 Shackleton, N.J., 2000. The 100,000-year ice-age cycle identified and found to lag temperature, carbon
942 dioxide, and orbital eccentricity. Science 289, 1897–1902.
943 https://doi.org/10.1126/science.289.5486.1897
944 Shackleton, N.J., 1987. Oxygen isotopes, ice volume and sea level. Quat. Sci. Rev. 6, 183–190.
945 Shackleton, N.J., 1969. The last interglacial in the marine and terrestrial records. Proc. R. Soc. London. Ser.
946 B. Biol. Sci. 174, 135–154.
947 Shackleton, N.J., Sánchez-Goñi, M.F., Pailler, D., Lancelot, Y., 2003. Marine isotope substage 5e and the
948 Eemian interglacial. Glob. Planet. Change 36, 151–155. https://doi.org/10.1016/S0921-8181(02)00181-
949 9
950 Siddall, M., Rohling, E.J., Almogi-Labin, A., Hemleben, C., Meischner, D., Schmelzer, I., Smeed, D.A.,
951 2003. Supplementary Information: Sea-level fluctuations during the last glacial cycle. Nature 423, 0–5.
952 https://doi.org/10.1038/nature01687.1.

Stammer, D., Wal, R.S.W., Nicholls, R.J., Church, J.A., Le Cozannet, G., Lowe, J.A., Horton, B.P., White, K., Behar, D., Hinkel, J., 2019. Framework for High-End Estimates of Sea Level Rise for Stakeholder Applications, Earth's Future. https://doi.org/10.1029/2019ef001163

Tanabe, S., Nakanishi, T., Matsushima, H., Hong, W., 2013. Sediment accumulation patterns in a tectonically subsiding incised valley: Insight from the Echigo Plain, central Japan. Mar. Geol. 336, 33–43. https://doi.org/10.1016/j.margeo.2012.11.006

Tanabe, S., Saito, Y., Lan Vu, Q., Hanebuth, T.J.J., Lan Ngo, Q., Kitamura, A., 2006. Holocene evolution of the Song Hong (Red River) delta system, northern Vietnam. Sediment. Geol. 187, 29–61. https://doi.org/10.1016/j.sedgeo.2005.12.004

Tanabe, S., Tateishi, M., Shibata, Y., 2009. The sea-level record of the last deglacial in the Shinano River incised-valley fill, Echigo Plain, central Japan. Mar. Geol. 266, 223–231. https://doi.org/10.1016/j.margeo.2009.08.011

Törnqvist, T.E., Wallinga, J., Murray, A.S., De Wolf, H., Cleveringa, P., De Gans, W., 2000. Response of the Rhine-Meuse system (west-central Netherlands) to the last Quaternary glacio-eustatic cycles: A first assessment. Glob. Planet. Change 27, 89–111. https://doi.org/10.1016/S0921-8181(01)00072-8

Toscani, G., Bonini, L., Ahmad, M.I., Bucci, D. Di, Giulio, A. Di, Seno, S., Galuppo, C., 2014. Opposite verging chains sharing the same foreland: Kinematics and interactions through analogue models (Central Po Plain, Italy). Tectonophysics 633, 268–282. https://doi.org/10.1016/j.tecto.2014.07.019

Tropeano, M., Cilumbriello, A., Sabato, L., Gallicchio, S., Grippa, A., Longhitano, S.G., Bianca, M., Gallipoli, M.R., Mucciarelli, M., Spilotro, G., 2013. Surface and subsurface of the Metaponto Coastal Plain (Gulf of Taranto-southern Italy): Present-day- vs LGM-landscape. Geomorphology 203, 115–131. https://doi.org/10.1016/j.geomorph.2013.07.017

Tzedakis, C., 2013. Pollen Records, Last Interglacial of Europe, 2nd ed, Encyclopedia of Quaternary Science: Second Edition. Elsevier B.V. https://doi.org/10.1016/B978-0-444-53643-3.00183-7

Tzedakis, P.C., Drysdale, R.N., Margari, V., Skinner, L.C., Menviel, L., Rhodes, R.H., Taschetto, A.S., Hodell, D.A., Crowhurst, S.J., Hellstrom, J.C., Fallick, A.E., Grimalt, J.O., McManus, J.F., Martrat, B., Mokeddem, Z., Parrenin, F., Regattieri, E., Roe, K., Zanchetta, G., 2018. Enhanced climate instability in the North Atlantic and southern Europe during the Last Interglacial. Nat. Commun. 9.

https://doi.org/10.1038/s41467-018-06683-3

Vis, G.J., Kasse, C., Vandenberghe, J., 2008. Late Pleistocene and Holocene palaeogeography of the Lower Tagus Valley (Portugal): effects of relative sea level, valley morphology and sediment supply. Quat. Sci. Rev. 27, 1682–1709. https://doi.org/10.1016/j.quascirev.2008.07.003

Waelbroeck, C., Labeyrie, L., Michel, E., Duplessy, J.C., McManus, J.F., Lambeck, K., Balbon, E., Labracherie, M., 2002. Sea-level and deep water temperature changes derived from benthic foraminifera isotopic records. Quat. Sci. Rev. 21, 295–305.

Wintle, A.G., Murray, A.S., 2006. A review of quartz optically stimulated luminescence characteristics and their relevance in single-aliquot regeneration dating protocols. Radiat. Meas. 41, 369–391.